Comparative analysis of mass balance estimates since 1959 at Mittivakkat Gletsjer (SE Greenland)

Journal:	*Journal of Glaciology*
Manuscript ID	JOG-2025-0164.R1
Manuscript Type:	Article
Date Submitted by the Author:	n/a
Complete List of Authors:	Posch, Christoph; University of Graz, Department of Geography and Regional Science; University of Lausanne, Institute of Earth Surface Dynamics de Villiers, Simon; Western Norway University of Applied Sciences - Sogndal Campus, Department of Civil Engineering and Environmental Sciences Sjursen, Kamilla ; Western Norway University of Applied Sciences - Sogndal Campus, Department of Civil Engineering and Environmental Sciences Yde, Jacob; Western Norway University of Applied Sciences - Sogndal Campus, Department of Civil Engineering and Environmental Sciences Bjørk, Anders; Københavns Universitet, Department of Geoscience and Natural Resource Management Gillespie, Mette; VIA University College, Teachers Education; Western Norway University of Applied Sciences - Sogndal Campus, Department of Civil Engineering and Environmental Sciences Knudsen, Niels; Aarhus Universitet, Department of Geoscience Noël, Brice; University of Liege, Department of Geography, Laboratory of Climatology, SPHERES research unit Schöner, Wolfgang; University of Graz, Department of Geography and Regional Science Abermann, Jakob; University of Graz, Department of Geography and Regional Science

Keywords:	Glacier mass balance, Surface mass budget, Mass-balance reconstruction, Arctic glaciology, Glacier fluctuations
Abstract:	Mittivakkat Gletsjer (MIT) has the longest glaciological surface mass balance (SMB) record of any peripheral glacier in Greenland. In this study, we utilize the glaciological SMB record, calibrate SMB from the Regional Atmospheric Climate Model (RACMO), and calculate geodetic mass balance (MB) to provide a multi-methodic assessment of trends in SMB. Glaciological SMB and modelled SMB correlate well ($r = 0.80$, $p < 0.01$) and all three methods agree on an accelerating mass loss. The modelled output shows that mass loss more than tripled from -0.26 ± 0.40 m w.e. a^{-1} on average in 1959-92 to -0.91 ± 0.40 m w.e. a^{-1} in 1993-2024, coinciding with an annual mean temperature increase from -1.6°C to -0.1°C for the respective periods. The modelled SMB extending back to 1959 shows that mass loss is linked to increasing air temperatures and decreasing winter precipitation. Our findings highlight: (I) Calibrating SMB from RACMO allows for reconstructing mass changes on the scale of individual glaciers. (II) MIT is out of balance with the current climate and experienced a change in mass balance during the 1990s, similar to that observed in the Greenland periphery.

Note: The following files were submitted by the author for peer review, but cannot be converted to PDF. You must view these files (e.g. movies) online.

MIT_MB_figures.zip

Comparative analysis of mass balance estimates since 1959 at Mittivakkat Gletsjer (SE Greenland)

Christoph Posch[1,2], Simon de Villiers[3], Kamilla Hauknes Sjursen[3], Jacob Clement Yde[3], Anders Anker Bjørk[4], Mette Kusk Gillespie[3,5], Niels Tvis Knudsen[6], Brice Noël[7], Wolfgang Schöner[1], Jakob Abermann[1]

[1] Department of Geography and Regional Science, University of Graz, Graz, Austria
[2] Institute of Earth Surface Dynamics, University of Lausanne, Lausanne, Switzerland
[3] Department of Civil Engineering and Earth Sciences, Western Norway University of Applied Sciences, Sogndal, Norway
[4] Department of Geoscience and Natural Resource Management, University of Copenhagen, Copenhagen, Denmark
[5] Teachers Education, VIA University College, Nørre Nissum, Denmark
[6] Department of Geoscience, Aarhus University, Aarhus, Denmark
[7] Laboratory of Climatology, Department of Geography, SPHERES research unit, University of Liège, Liège, Belgium

Corresponding author: Christoph Posch (christoph.posch@unil.ch)

ABSTRACT

Mittivakkat Gletsjer (MIT) has the longest glaciological surface mass balance (SMB) record of any peripheral glacier in Greenland. In this study, we utilize the glaciological SMB record, calibrate SMB from the Regional Atmospheric Climate Model (RACMO), and calculate geodetic mass balance (MB) to provide a multi-methodic assessment of trends in SMB. Glaciological SMB and modelled SMB correlate well ($r = 0.80$, $p < 0.01$) and all three methods agree on an accelerating mass loss. The modelled output shows that mass loss more than tripled from -0.26 ± 0.40 m w.e. a^{-1} on average in 1959-92 to -0.91 ± 0.40 m w.e. a^{-1} in 1993-2024, coinciding with an annual mean temperature increase from -1.6°C to -0.1°C for the respective periods. The modelled SMB extending back to 1959 shows that mass loss is linked to increasing air temperatures and decreasing winter precipitation. Our findings highlight: (I) Calibrating SMB from RACMO allows for reconstructing mass changes on the scale of individual glaciers. (II) MIT is out of balance with the current climate and experienced a change in mass balance during the 1990s, similar to that observed in the Greenland periphery.

1. INTRODUCTION

Glacier mass change is directly linked to atmospheric and ice surface processes. Projecting glacier response to future climate change is of great importance to assess their contribution to sea level rise, glacier-related hazards, and environmental impacts. Glacier mass loss affects local hydrology and downstream ecosystems as mass is generally lost through meltwater runoff (Kaser and others, 2003). Globally, the great majority of Greenland peripheral glaciers and ice caps (GICs) have been losing mass in the last decades (Hugonnet and others, 2021; Dussaillant and others, 2025), translating to a global mean sea level rise estimate of 17.1 ± 4.4 mm during 1993-2019, and they will continue to do so as a result of climate warming (IPCC, 2021,2022). Since 1979, annual mean air temperatures in the Arctic (66.5-90 °N) have increased nearly four times faster than the global average (Rantanen and others, 2022). Glaciers across the Arctic have shown to contribute to global sea level rise in the same magnitude as the Greenland Ice Sheet (GrIS), while their specific (per unit area) mass loss was larger (Box and others, 2018). Peripheral glaciers in Greenland contributed 13 % to the global glacier mass loss between 2000-19 (Hugonnet and others, 2021) and have shown largest mass losses when compared to other Arctic glaciers during 2006-15 (IPCC, 2019). In Greenland, both summer and winter mean temperatures increased significantly between 1991 and 2019 (Hanna and others, 2021),

coinciding with accelerating mass loss of Greenland glaciers in recent decades (Carrivick and others, 2023; Khan and others, 2022; Larocca and others, 2023; The GlaMBIE Team, 2025).

Mittivakkat Gletsjer (MIT) is a peripheral glacier located in southeast Greenland (Fig. 1). It has exhibited a significant glacier frontal retreat and surface lowering since the 1930s (Knudsen and Hasholt, 2008). Climate-forced changes in the glacier area and volume of MIT are well-documented (Knudsen and Hasholt, 1999; Mernild and others, 2011) and several studies have focused on its mass evolution since the initiation of the glaciological mass balance program in 1995 (i.e., Knudsen and Hasholt, 1999, 2004, 2008; Mernild and others, 2008a, 2008b, 2011, 2013a, 2013b, 2018; Yde and others, 2014). Since 1995, most of the years documented in the glaciological mass balance record have shown net mass losses (WGMS, 2025) and MIT is expected to continue losing mass in the future (Mernild and others, 2011).

With a high-quality SMB time series of several decades that is the longest for any peripheral glaciers in Greenland, we can showcase several relevant scientific avenues: I) Using regional climate model outputs, we can assess the potential of reproducing mass balance variability for unmeasured areas. II) Provided this is successful, we can extend the time series to the past and use selected historical elevation models for validation. III) Using our reconstructed mass balance series, we can identify drivers of mass changes and relate them to circulation anomalies. In that respect, this study aims to compare glaciological, modelled, and geodetic data to evaluate trends in the mass balance of MIT during the period 1959-2024. To reconcile mass changes on MIT across different data sources, we utilize the ablation and accumulation stake records (glaciological surface mass balance), estimates from the Regional Atmospheric Climate Model (RACMO2.3p2) (modelled surface mass balance) statistically downscaled to 1 km resolution, and mass losses estimate from volume changes derived from digital elevation models (DEMs) using a density conversion (geodetic mass balance). The agreement and magnitude of the mass balances independently estimated by the three methods are compared and trends in MIT mass changes are discussed based on climate indices and previous studies.

2. STUDY AREA

Mittivakkat Gletsjer is a temperate glacier (Knudsen and Hasholt, 1999) on the island Ammassalik Ø in south-east Greenland located approximately at 65.70 °N and 37.80 °W (Fig. 1). The volume of MIT was about 1.44 km^3 in 2012 (Yde and others, 2014) and the surface area roughly covered 16 km^2 in summer 2023. The glacier is situated about 50 km east of the eastern GrIS margin, separated from the mainland by the 10-15 km wide Sermilik Fjord, and approximately 15 km northwest of the town Tasiilaq. In 2023, the altitudinal extent of the glacier ranged from 160 m a.s.l. to 930 m a.s.l. and the mean surface slope was estimated at 5.9° in 2011 (Mernild and others, 2018). The main part of the glacier flows towards the west, while towards the south and east it is constrained by mountain ridges. The northern glacier margin mainly consists of several protruding. The glacier bedrock consists of granite-gneiss (Bridgwater, 1976) and unconsolidated subglacial sediments that are only observed sporadically along the ice margin. The area is characterized by a Low Arctic tundra climate, representing a relatively humid part of Greenland (Mernild and others, 2015a). Climatological data for 1991-2020 from the meteorological station in Tasiilaq reported by Capellen and Jensen (2021) shows that the mean annual air temperature is -0.3 °C (Hansche and others, 2023), while the mean annual wind speed reported by Station Coast in MIT vicinity is approximately 4 m s^{-1} (Mernild and others, 2006a; Mernild and others, 2008b).

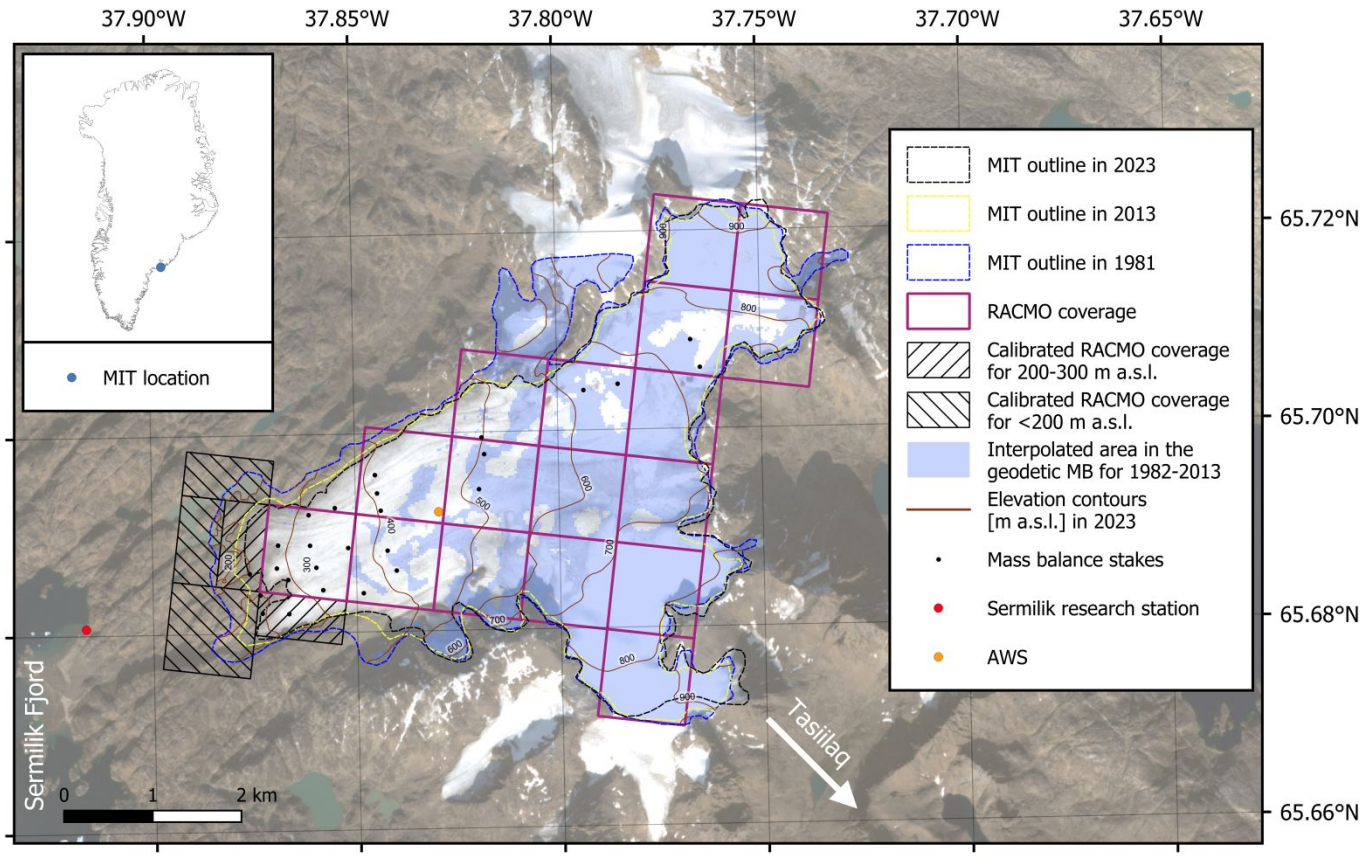

Fig. 1. Overview map of the Mittivakkat Gletsjer (MIT). Elevation contours in 100 m-intervals are derived from the Pléiades DEM in 2023. The MIT outlines used for the geodetic mass balance are digitized from orthoimages of the AERODEM (Korsgaard and others, 2016a) and Pléiades DEM and from Landsat 7 imagery (USGS, 2024) acquired on 20130803. Locations are shown for mass balance stakes which are currently utilized within the glaciological mass balance programme. The fixed RACMO coverage (purple) corresponds to the uncalibrated model output. The calibrated model output is based on the fixed RACMO coverage and the calibrated coverage for 200-300 m a.s.l. and <200 m a.s.l. The RACMO glacier mask area for 200-300 m a.s.l. is decreased by 0.03 km^2 a^{-1} from 1959-2024 to account for the glacier retreat (see Methods section). Background image: S2 scene from 20230915 (ESA 2025). Overview map: Greenland outline from QGreenland (2024), modified from Natural Earth (2024).

3. RESEARCH HISTORY

Mittivakkat Gletsjer is one of Greenland's most intensively studied glaciers. Since 1933, MIT has been observed at irregular intervals by means of field observations, aerial photography, and satellite imagery (Hasholt and Jakobsen, 2013; Mernild and others, 2015b). Based on the earliest scientific glacier work on MIT in that year, conducted by the geologist Keld Milthers, it was picked as one of the Danish focus sites for Arctic research during the International Geophysical Year (IGY) 1957/58 (Fristrup, 1970). The first mass change studies were conducted by Fristrup (1960), showing that the glacier retreated since 1933 (Fristrup, 1970; Hasholt and others, 2016). Since then, MIT and the surrounding landscape have been photographed and changes of glacier extent are well-documented (e.g., Knudsen and Hasholt, 1999; Mernild and others, 2011). Historical topographic maps have been issued based on photogrammetric surveys conducted in 1933, 1972, and 1981 (Hasholt, 1986; 1987). The glacier retreat has been most pronounced along the western and northern margins (Knudsen and Hasholt, 1999). Until about 1969, the glacier mainly retreated across a flat alluvial plain and then up through steep and narrow gorges (Knudsen and Hasholt, 2008). The retreat of the terminus has been influenced by the transition from valley to peak topography as the terminus has moved inland

from the fjord, by climate variability, and by ice dynamic processes (Mernild and others, 2011). Volume and ice thickness estimates and their change rates have been determined by two radar surveys in 1994 and 2012 (Knudsen and Hasholt, 1999; Yde and others, 2014).

As a result of harsh climate conditions and logistical difficulties, few reliable long-term observations of mass loss and glacier retreat are available for Greenland's peripheral glaciers. In 1995, the current glaciological SMB program at MIT was initiated by Niels Tvis Knudsen and later continued by Simon de Villiers (Mernild and others, 2011). Before the initiation of the SMB program, mass changes were estimated from photogrammetric and topographic surveys and maps (Knudsen and Hasholt, 2004, 2008). More recently, geodetic mass balance for Greenland's peripheral glaciers, including MIT, have been estimated using space-borne digital elevation models (Hugonnet and others, 2021; Dussailant and others, 2025). Since 2009, an automated weather station (AWS) located at 65.69 °N, 37.83 °W, 440 m a.s.l. (PROMICE/GC-NET, 2024) records surface ablation and meteorological conditions. The AWS is located below the long-term equilibrium line altitude (ELA), resulting on average in a negative specific net mass balance at the AWS site (Fausto and others, 2020). Since the early 2000s, about 20 studies have been discussing mass balance at MIT. Knudsen and others (2008) discussed MIT retreat based on radiocarbon dating of reindeer and polar bear remains, and peat material. Mernild and others (2015) focused on albedo at the MIT surface, which exhibits mainly windblown sediment and englacially transported debris. They found that glacier-wide albedo has been declining between 2000 and 2013. Other studies, focused on snow melt simulations, discharge, and internal drainage systems, addressed the MIT drainage system efficiency and found increasing runoff and discharge quantities (Mernild, 2006; Mernild and Hasholt, 2006; Mernild and others, 2006a, 2006b). Studies on the MIT area climate have been using meteorological data from the AWS installed on the glacier as part of the PROMICE/GC-NET (2024) network (Fig. 1), two periglacial AWSs in the glacier vicinity, and one AWS located in Tasiilaq. The two periglacial stations, i.e., Nunatak (65.710 °N, 37.812 °W, 515 m a.s.l.) and Coast (65.680 °N, 37.917 °W, 25 m a.s.l.), recorded meteorological conditions since 1993 and 1997, respectively, and showed increasing air temperatures (Mernild and others, 2008a, 2008c).

4. DATA

4.1 Mass balance stake record

To estimate glaciological SMB and calibrate our model, we utilize annual specific and elevation-band SMB compiled in the Fluctuation of Glacier Database Version 2024 (WGMS, 2025). Fig. 1 shows the locations of mass balance stakes at MIT, which are currently, or were until recently, part of the glaciological SMB program. The number of stakes varies with time and has been reduced after about 2011 (Mernild and others, 2013a), partly due to glacier retreat. The mass balance stakes cover major parts of the ablation area and the northern parts of the accumulation area. Due to a high density of crevasses in the south-eastern part of the glacier, no stakes were installed for the mass balance program there.

4.2 Regional Atmospheric Climate Model

We utilize monthly cumulative modeled SMB from the Regional Atmospheric Climate Model (RACMO) covering the Mittivakkat region from January 1958 to December 2024 (Noël and others, 2019). RACMO is a regional atmospheric climate model forced by meteorological reanalysis data (van Meijgaard and others, 2008). The current operational version RACMO2.3p2 – for simplicity, hereafter referred to as 'RACMO' – is an adapted version for high latitudes with a spatial resolution of 5.5 km.

The dynamical core of the High-Resolution Limited Area Model (HIRLAM) (Undèn and others, 2002) and the physics package cycle CY33r1 of the European Centre for Medium-Range Weather Forecasts Integrated Forecast System (ECMWF-IFS, 2008) are incorporated in RACMO. A multilayer snow module that simulates melting, liquid-water percolation and retention, refreezing, and runoff (Ettema and others, 2010) is included. Dry snow densification (Ligtenberg and others, 2011) and drifting snow erosion and sublimation (Lenaerts and others, 2012) are accounted for. An albedo scheme calculating snow albedo based on prognostic snow grain size, cloud optical thickness, solar zenith angle, and impurity concentration in snow (Kuipers Munneke and others, 2011) is included (Noël and others, 2018).

In the model, melt energy flux is estimated by closing the surface energy budget. Consequently, SMB is estimated from precipitation, sublimation from drifting snow and surface processes, erosion from drifting snow, and runoff (Noël and others, 2018). RACMO is evaluated against 37 AWSs on and around the GrIS, including the supraglacial Mittivakkat AWS, and is shown to realistically represent near-surface temperature, specific humidity, wind speed and air pressure ($0.73 < R^2 < 0.98$), and cloud conditions through shortwave and longwave radiation components ($0.85 < R^2 < 0.96$) (Noël and others 2019). This translates to biases of 0.14 °C for daily mean air temperatures at 2 m, -0.11 g kg^{-1} for specific humidity, and 4.3 W m^{-2} and -7.8 W m^{-2} for shortwave and longwave radiation, respectively. Modeled SMB has been evaluated using mass balance stake measurements at 182 sites in the accumulation zone and 1073 stake measurements at 213 sites in the ablation zone of the GrIS and shows good agreement ($R^2 = 0.78$) (Noël and others 2019). The data we use have been statistically downscaled to 1 km resolution. This high resolution is essential to resolve the narrow ablation zone and marginal glacier tongues in sufficient detail (Noël and others, 2019). The RACMO simulations used in this study have been forced with reanalysis data from ERA40 (ECMWF, 2024a) for 1958-78, ERA-Interim (ECMWF, 2024b) for 1979-89, and ERA5 (ECMWF, 2024c) for 1990-2024.

4.3 Digital elevation models

4.3.1 AERODEM

AERODEM (Korsgaard and others, 2016a) is a 25 x 25 m gridded DEM including a 2 m resolution orthophotograph derived from approximately 3500 vertical photographs acquired from 1978-87 that cover the coastal regions of Greenland and a significant part of the GrIS margin. The product is based on aero-triangulation and validated as described in Kjeldsen and others (2015) following co-registration methods described in Kääb and others (2005) and Nuth and Kääb (2011) (Korsgaard and others, 2016b). In this study, we utilize the data product of the section UTM 24N. The aerial images which serve as basis for the DEM and orthophotograph in the Mittivakkat area were acquired in 1981. The DEM shows to be accurate to 10 m horizontally and 6 m vertically (Korsgaard and others, 2016a).

4.3.2 ArcticDEM

ArcticDEM (Porter and others, 2018) is a high-resolution and high-quality DEM of the Arctic using optical stereo imagery, high-performance computing, and open-source photogrammetry software. It is based on imagery from the high-resolution Maxar (2024) satellite systems including WorldView-1, WorldView-2, and WorldView-3, and GeoEye-1, acquired over the summer seasons between 2007 and 2022. ArcticDEM is produced from processed stereoscopic images using the Surface Extraction by TIN-based Search Space Minimization (SETSM) method (Noh and Howat, 2015). The coverage of ArcticDEM includes land areas north of 60 °N and the entirety of Greenland. In this study, we utilize ArcticDEM strip data from 20130730. The absolute accuracy of ArcticDEM is evaluated by the SETSM

method (Noh and Howat, 2015) and is approximately 4 m in horizontal and vertical directions (PGC, 2024).

4.3.3 Pléiades DEM

The Pléiades satellite mission, launched in 2011/12, acquires high-resolution imagery in a sun-synchronous orbit at an altitude of 694 km (CNES, 2024a). In this study, we utilize the Pléiades product including DEMs and orthoimages from 20230809 and 20230810. The DEMs and orthoimages have been generated from Pléiades images using the NASA Ames Stereo Pipeline (ASP) (Beyer and others, 2018). The set of processing parameters used for DEM generation based on semi-global matching are from Deschamps-Berger and others (2020). The DEMs and orthoimages are co-registered to the GLO-30 DEM (ESA, 2024) using the 'demcoreg' tool (Shean and others, 2021). Pléiades DEMs, which have been computed without ground control points (GCPs), exhibit vertical and horizontal inaccuracies of ± 5-10 m (Berthier and others, 2024).

4.4 Meteorological observations

We use 2 m air temperature and accumulated precipitation data from the station Tasiilaq to relate the SMB evolution to the temperature and precipitations trend since 1958. The Tasiilaq weather station is approximately 15 km southeast of MIT and the data is provided by the Danish Meteorological Institute (DMI, 2026).

4.5 Climate indices

We utilize data of the North Atlantic Oscillation (NAO) (Barnston and Livezey, 1987), Greenland Blocking Index (GBI) (Hanna and others, 2016), Atlantic Multi-decadal Oscillation (AMO) (Enfield and others, 2001), and sea surface temperature (SST) anomaly (Kaplan and others, 1998) for the period 1959-2022 to identify links with MIT surface mass balance on a larger scale. The NAO index and GBI are annual index values for the summer months June-August and the AMO index and SST anomalies represent standardized annual temperature anomalies (NOAA CPC, 2024; NOAA PSL, 2024a, 2024b, 2024c). While the AMO index represents the SST variability across the North Atlantic Ocean, we also utilize local SST anomaly data derived from a grid cell in the vicinity of Ammassalik Island that is closest to MIT (Fig. S1).

Negative NAO index values are caused by the weakening of the pressure gradient between the Azores High and the Icelandic Low and are typically associated with higher temperatures over Greenland leading to increased summer melt. In contrast, positive NAO index values are associated with reinforced westerlies, storm track activity, and lower temperatures over Greenland (Bjørk and others, 2018, Silva and others, 2022). GBI represents the mean 500 hPa geopotential height for the 60-80 °N, 20-80 °W region (Hanna and others, 2016) and is strongly correlated with surface air temperature data from coastal Greenland and GrIS runoff since the 1970s, making it a potentially useful predictor of GrIS mass balance changes (Hanna and others, 2012). AMO is the leading low-frequency (multi-decadal) mode of sea surface temperature computed as area weighted averages over the North Atlantic (0-70 °N) (Hanna and others, 2012; NOAA PSL, 2024b) and is significantly correlated with Greenland temperatures and GrIS runoff (Hanna and others, 2012).

5. METHODS

5.1 Glaciological surface mass balance

The uncertainty in annual glacier-wide mass balance from the glaciological record of MIT has been estimated to ± 15 % (Mernild and others, 2011). Using this measure, uncertainties in annual mass balance over the period 1996-2024 vary between ± 0.06 and ± 0.32 m w.e. annually, with a median value of ± 0.18 m w.e. Huss and others (2017) estimate that uncertainties in annual mass balance for glaciers in the Swiss Alps range from ± 0.15 to ± 0.40 m w.e. Further, they consider the uncertainty to be close to the lower bound of this range for glaciers with a dense network of stake measurements. Therefore, we assume the uncertainty in the annual glacier-wide mass balance at MIT to be of similar magnitude and assign a fixed value of ± 0.32 m w.e., corresponding to the largest uncertainty as estimated by Mernild and others (2011).

5.2 Modelled surface mass balance

We tested different configurations combining several mass-balance year definitions (Jan–Dec, Sep–Aug, and Oct–Sep) and RACMO grid-cell coverages (Fig. S2) for MIT, and compared the resulting annual specific SMB estimates for 1996–2024 with the glaciological record. For our analysis, we selected the Sep-Aug mass-balance year from RACMO, as it aligns with the period used in the glaciological data. Furthermore, we found that using a minimal grid cell coverage over the glacier (Fig. S2d), corresponding to the RACMO coverage shown in Fig. 1, yielded the strongest relationship (R^2 = 0.82, p < 0.01) with the glaciological record. This configuration, however, underestimates the glacier-wide mass loss by approximately 39 % for 1996-2024. RACMO uses a fixed glacier mask at 1 × 1 km resolution and only partially covers MIT. The fixed glacier mask ignores past glacier extents at low elevations where the terminus has retreated several kilometers over the last decades. This introduces a significant bias in glacier-wide modelled SMB estimates. As a result, temporal changes in glacier area must be introduced via additional ice-mask adjustments. In this study, we therefore present two modelled SMB outputs following the workflow shown in Fig. 2: (I) Uncalibrated modelled SMB, which corresponds to the fixed spatial model coverage (Fig. 1) that covers an elevation range between 300 m a.s.l. and >800 m a.s.l. (II) Calibrated modelled SMB, which accounts for glacier surface area changes by expanding the modelled area at the lower ablation zone based on observed glacier change rates (Fig. 1). As the area reconstruction includes elevations that are lower and outside the fixed glacier mask domain, SMB for elevations <300 m a.s.l. are estimated by following method:

(I) We use polynomial regression to relate SMB in the two lowest elevation bands (<200 m a.s.l. and 200-300 m a.s.l.) to SMB in the higher elevation bands (300-400, 400-500, 500-600, 600-700, and >800 m a.s.l.) using the glaciological elevation-band record. The period 1996-2010 serves as training data (n = 15), and 2011-2024 as validation data (n = 12). SMB in the <200 m ($\overline{b_1}$) and 200–300 m ($\overline{b_2}$) elevation bands are estimated using Eq. (1) and Eq. (2),

$$\overline{b_1} = 1.53\,\overline{b_3} - 0.91\,\overline{b_4} - 1.70\,\overline{b_5} + 2.25\,\overline{b_6} + 0.45\,\overline{b_7} - 0.42\,\overline{b_8} - 1.92 \quad \text{Eq. (1)}$$

$$\overline{b_2} = 1.70\,\overline{b_3} - 0.96\,\overline{b_4} - 0.94\,\overline{b_5} + 1.57\,\overline{b_6} + 0.02\,\overline{b_7} - 0.35\,\overline{b_8} - 0.70 \quad \text{Eq. (2)}$$

where $\overline{b_3}$, $\overline{b_4}$, $\overline{b_5}$, $\overline{b_6}$, $\overline{b_7}$, and $\overline{b_8}$ correspond to the 100 m-elevation bands of the glaciological SMB between 300-700 and >800 m a.s.l., respectively. The relationships shown in Eq. (1) and Eq. (2) show strong correlations (R^2 = 0.93 and R^2 = 0.98, respectively) and in both cases $\overline{b_3}$ proves to be the significant predictor (p = 0.05 and p < 0.01, respectively). Comparison of predicted $\overline{b_1}$ and $\overline{b_2}$ during

the validation period demonstrates that SMB in the lowest elevation bands can be reliably inferred from SMB at higher elevations ($R^2 = 0.60$, $p < 0.01$ and $R^2 = 0.88$, $p < 0.01$, respectively). (II) We use the relationships derived from the glaciological record on the RACMO output, taking the model's higher-elevation band SMB (300-400, 400-500, 500-600, 600-700, and >800 m a.s.l.) as inputs to predict modelled SMB in the <200 m and 200–300 m bands. (III) We add two 500 m × 1 km grid cells to the RACMO domain, based on visual inspection of the 2023 glacier outline, to account for the today's (2023) glacier surface area. This added coverage corresponds to SMB in the 200-300 m a.s.l. elevation band. To account for glacier surface-area changes in the reconstructed SMB series back to 1959 beyond that reconstructed 2023 margin, we assume that SMB at <200 m a.s.l. represents the retreating MIT tongue as the today's pro-glacial terrain exhibits negligible elevation changes. Glacier area loss between 1981 and 2022, derived from AERODEM and Pléiades orthophotos, amounts to 1.30 km^2. We expand the model domain by growing the <200 m SMB area coverage by 0.03 km^2 yr^{-1}, corresponding to a total area loss of 2.04 km^2 since 1959. A conceptual illustration of the added RACMO coverage is shown in Fig. 1.

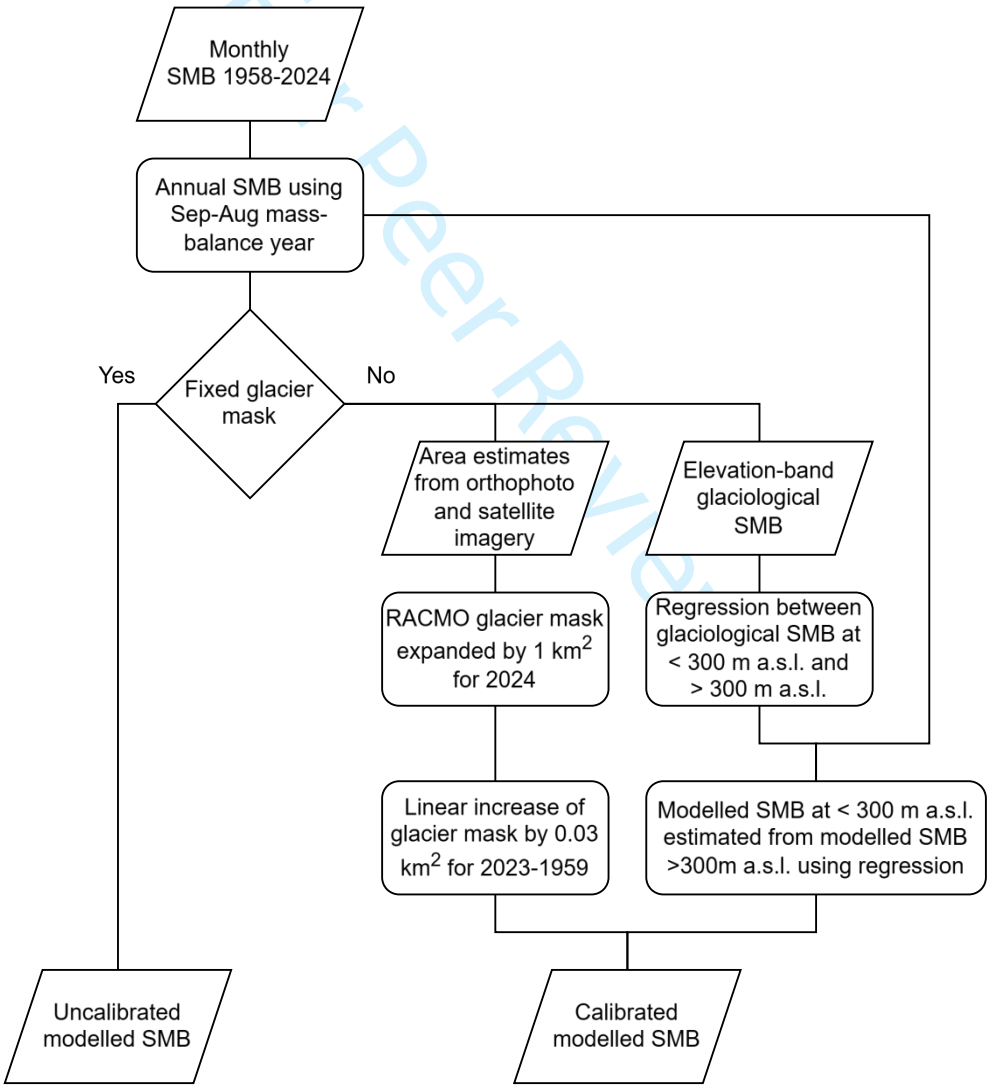

Fig. 2. Flowchart showing the processing steps for the modelled SMB estimates from RACMO. The two outputs in this study consist of the uncalibrated modelled SMB which uses the fixed glacier mask of the initial RACMO coverage and the calibrated modelled SMB which accounts for former glacier extents and estimates SMB at low elevations from SMB at higher elevation bands.

In addition to the ice-mask adjustment for the model output in the lower ablation area, we tested the sensitivity of modelled estimates to adjusting the higher-elevation SMB grid-cell coverage to match the digitized outlines. Calibrating the SMB coverage in these elevation bands (300-400, 400-500, 500-600, 700-800, and >800 m a.s.l.) did not significantly affect the resulting specific SMB ($p > 0.05$). We therefore chose not to apply area calibrations in these sections. RACMO SMB estimates have an uncertainty of ±0.40 m w.e., based on evaluation against stake measurements across the GrIS (Noël et al., 2019), and we adopt this uncertainty for both the uncalibrated and calibrated RACMO SMB used in this study.

5.3 Geodetic mass balance

To estimate the geodetic mass balance at MIT, we use DEM products from AERODEM, ArcticDEM, and Pléiades corresponding to the acquisition years 1981, 2013, and 2023. The DEMs are spaced by at least one decade, which is recommended to enhance the climatic signal, minimize short-term elevation variability driven by seasonal or interannual meteorological conditions, and reduce uncertainties introduced by the volume-to-mass conversion (Huss, 2013; Zemp et al., 2013; Berthier et al., 2023). Pre-processing of the DEMs includes mosaicking, reprojection, resampling, and co-registration. We neglect the influence of snow cover in the ArcticDEM and Pléiades DEMs because both scenes were acquired during summer and contain little to no periglacial snow. In the AERODEM, approximately 60 % of the glacier surface elevations are interpolated due to low radiometric contrast over the high-elevation snow-covered areas (Korsgaard et al., 2016b). The workflow of the geodetic MB is shown in Fig. 3.

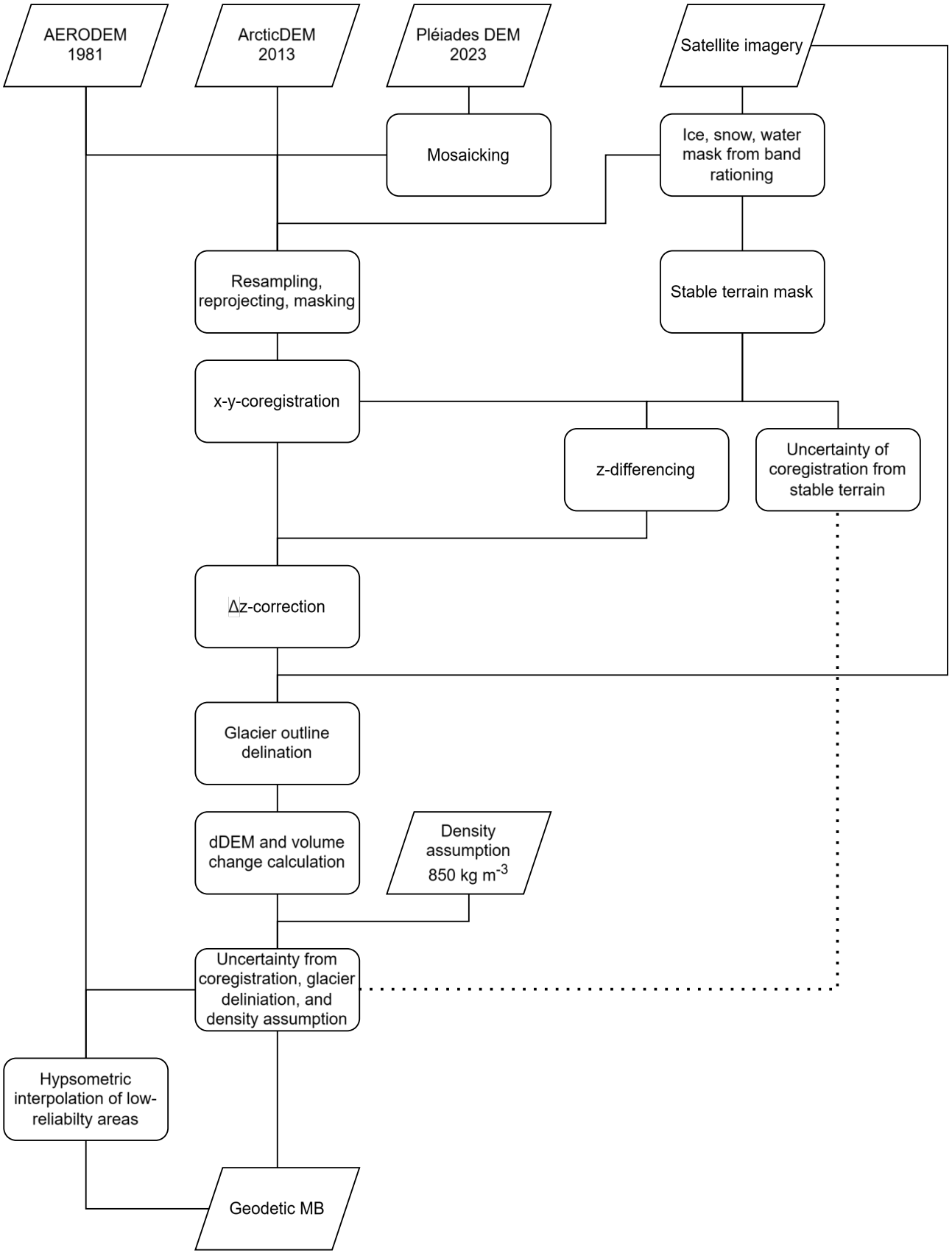

313

314 **Fig. 3.** Flowchart showing the processing steps for the geodetic MB estimates from AERODEM, ArcticDEM, and Pléiades
315 DEM. Geodetic MB is estimated from volume changes calculated from the x-y-z-coregistrated DEMs and an assumed density
316 conversion.

We co-register the DEMs in both the horizontal and vertical directions. For the horizontal co-registration, we use the *demcompare* algorithm (CNES, 2024b), which is based on Nuth and Kääb (2011), with the Pléiades DEM serving as the reference. Stable terrain is defined as all areas excluding ice, snow, and water, identified using the SWIR/red ratio of Sentinel-2 bands B11/B4 from the scene acquired on 2016-09-11, following the method of Paul et al. (2016). To account for temporal variations in water levels and ice extents, we apply a 500 m buffer around these excluded areas (Fig. S3). After horizontal (x–y) co-registration, we compute vertical differences over stable terrain and apply the modal offset as a vertical correction (Δz-correction). This results in vertical adjustments of 4.5 m for AERODEM and 3.7 m for ArcticDEM (Fig. S4, S5), aligning both datasets with the Pléiades DEM.

We manually digitized the glacier surface areas used for estimating geodetic mass balance from Pléiades and AERODEM orthoimagery, as well as from Landsat 7 imagery acquired on 2013-08-03 corresponding to the 2013 ArcticDEM (Fig. 1). As MIT is embedded within a larger glacier complex, we delineated its boundaries at the ice divides by interpreting elevation contours from the DEMs (Fig. S6). Following Zemp and others (2013), we estimate mass balance B_{geod} (m^3 w.e.) from differencing two DEMs multiplied by the ratio of an assumed glacier-wide density ρ (kg m^{-3}) and density of water ρ_w (kg m^{-3}) as shown in Eq. (3),

$$B_{geod} = \frac{\rho}{\rho_w} r^2 \sum_{k=1}^{K} \Delta h_k = \rho \Delta V \quad \text{Eq. (3)}$$

where ρ_w is the density of water, K is the number of pixels covering the glacier at the maximum extent, Δh_k is the elevation difference between the two grids at pixel k, and r is the pixel length (Zemp and others, 2013). Note that for calculating with K, Δh_k, k, and r, we resampled the three DEMs to a common geometric resolution. We convert volume change to mass change assuming a widely used density conversion of ρ = 850 kg m^{-3} (Huss, 2013). This is done for the MB period 2014-2023 using the ArcticDEM and Pléiades DEM since they show a comprehensive coverage of the glacier surface.

Due to the low reliability of AERODEM over approximately 60 % of the glacier surface, we interpolate mass changes t those low-reliability regions following the approaches introduced and evaluated by Kääb (2008) and McNabb et al. (2018). To estimate surface-elevation changes – and consequently volume and mass changes – between AERODEM and ArcticDEM, we apply a hypsometric interpolation method (*mean elevation difference by elevation bin interpolation*), which consists of the following steps: (I) We mask out low-reliability areas in AERODEM (Fig. 1). (II) We subtract AERODEM from ArcticDEM to create a DEM of Differences (dDEM) representing surface lowering between 1981 and 2013. (III) The dDEM is grouped into 50 m elevation intervals based on the elevations of the ArcticDEM, and the mean elevation difference is calculated for each interval. (IV) We then bin the full ArcticDEM surface into the same 50 m elevation bands which covers the entire MIT area coverage. For each band, volume change is computed by multiplying the bin area by the corresponding mean elevation difference derived from the dDEM. Finally, the geodetic mass balance B_{geod} (m^3 w.e.) is derived as shown in Eq. (4),

$$B_{geod} = \frac{\rho}{\rho_w} \sum_{j=1}^{J} S_j \overline{\Delta h_j} = \rho \Delta V \quad \text{Eq. (4)}$$

where J is the number of 50 m-elevation bins, $\overline{\Delta h_j}$ is the mean elevation difference of the dDEM in elevation bin j, and S_j is the area of the respective elevation bin.

Eventually, the specific mass balance ($\overline{b_{geod}}$) (m w.e.) can be denoted as shown in Eq. (5),

$$\overline{b_{geod}} = \frac{B_{geod}}{\overline{S}} = \frac{\rho \Delta V}{\overline{S}} \quad \text{Eq. (5)}$$

with $\overline{S} = \frac{S_{t0}+S_{t1}}{2}$

where $\overline{S}$ is the average glacier area of the two surveys at time $t0$ and $t1$, assuming a linear change through time (Zemp and others, 2013).

Three sources of uncertainty are considered in the geodetic mass balance: (I) The uncertainty introduced by manually delineating the glacier extent remained within ± 5 % of the total glacier area from the several attempts we performed. (II) The uncertainty related to the volume-to-mass conversion corresponds to the uncertainty in glacier-wide density, estimated at ± 60 kg m^{-3} (Huss, 2013). (III) The uncertainty introduced by the data and co-registration quality of the DEMs is assumed to correspond to the standard deviation of the vertical differences over stable terrain (Fig. S4, S5). From these three sources we estimate the total uncertainties in geodetic mass balance to be ± 0.36 m w.e. a^{-1} for 1982-2013 and ± 0.21 m w.e. a^{-1} for 2014-2023.

6. RESULTS

6.1 Mass balance at MIT

During 1996–2024, annual values from the calibrated model SMB are strongly correlated (r = 0.80, p < 0.01) with mass-loss estimates from the glaciological method (Fig. 4), while the uncalibrated output shows a weaker correlation (r = 0.61, p < 0.01). Our results also indicate that the calibrated model output lies within the uncertainty range of the cumulative reconstructions of both the geodetic mass balances and glaciological surface mass balance in the corresponding periods (Fig. 5c). Therefore, we find that the calibrated output captures mass evolution at MIT more confidently compared to the uncalibrated output, and we will therefore present and discuss the calibrated model output – hereinafter simply referred to as 'model/modelled SMB/output'.

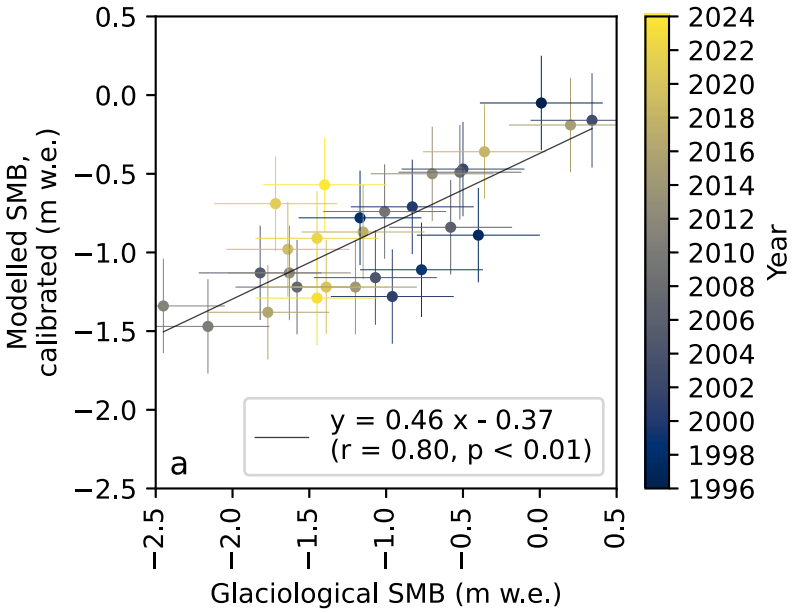

Fig. 4. a) Calibrated modelled SMB vs. glaciological SMB between 1996-2024, exhibiting a strong linear relationship (r = 0.80, p < 0.01). Vertical and horizontal lines represent uncertainties in the respective methods. b) Calibrated modelled SMB vs. 2 m mean air temperature in summer (Jun-Aug) in Tasiilaq (15 km NW southeast of MIT) between 1959-2024, exhibiting a moderately strong linear relationship (r = -0.39, p < 0.01).

The time series of the modelled output and the temperature record clearly show a shift in the mass balance and temperature regime during the mid-1990s (Fig. 5a,c). A two-sample t-test assuming unequal variances based on multiple sets of two SMB periods with varying break points during the 1990s (α = 0.05) showed a regime change in mass balance rates in 1992/1993. We found that mass balance rates show the largest differences in means as well as lowest p-values when comparing the periods 1959-92 and 1993-2024. We therefore discuss mass balance rates and temperature averages for those two periods hereafter.

Comparing the periods 1959-92 and 1993-2024, we find an average annual air temperature increase from -1.6 °C to -0.1 °C and average summer air temperature in Tasiilaq from 5.5 °C to 6.4 °C, respectively, coinciding with accelerated negative mass balance estimates in those periods (Table 1, Fig. 5a-d). Since 1959, the model output suggests a cumulative mass loss of 37.81 ± 26.40 m w.e. at MIT which translates to a SMB rate of -0.57 ± 0.40 m w.e. a^{-1} (Table 1, Fig. 5d). During 1959-92 and 1993-2024, SMB rates amount to -0.26 ± 0.40 m w.e. a^{-1} and -0.91 ± 0.40 m w.e. a^{-1}, respectively, indicating a tripling of mass loss between those two periods. Between 1996 and 2024, the glaciological SMB rate amounts to -1.07 ± 0.30 m w.e. a^{-1} while the calibrated modelled SMB rate amounts to -0.87 ± 0.40 m w.e. a^{-1}, highlighting a difference of mass change estimates of 20 % between those two methods. The geodetic mass balance rate for the period 1982-2023 amounts to -0.72 ± 0.33 m w.e. a^{-1} which is a specific mass change of -30.32 ± 14.07 m w.e. Geodetic mass changes are more negative during the period 2014-23 (-0.96 ± 0.21 m w.e. a^{-1}) compared to 1982-2013 (-0.65 ± 0.37 m w.e. a^{-1}). For the period 1982-2013, the modelled SMB rate agrees well with the geodetic MB rate, showing specific mass changes of -22.78 ± 13.20 m w.e. (modelled SMB) and -20.69 ± 11.98 m w.e. (geodetic MB). Rates of the modelled SMB agree well with the MB rate of the geodetic method during 2014-23, while all three methods highlight the accelerated mass loss at MIT during

that period (Table 1, Fig. 5c,d). The geodetic MB deviates by 19 % from the glaciological record in 2014-23, while the modelled SMB differs by 24 % compared to the glaciological SMB.

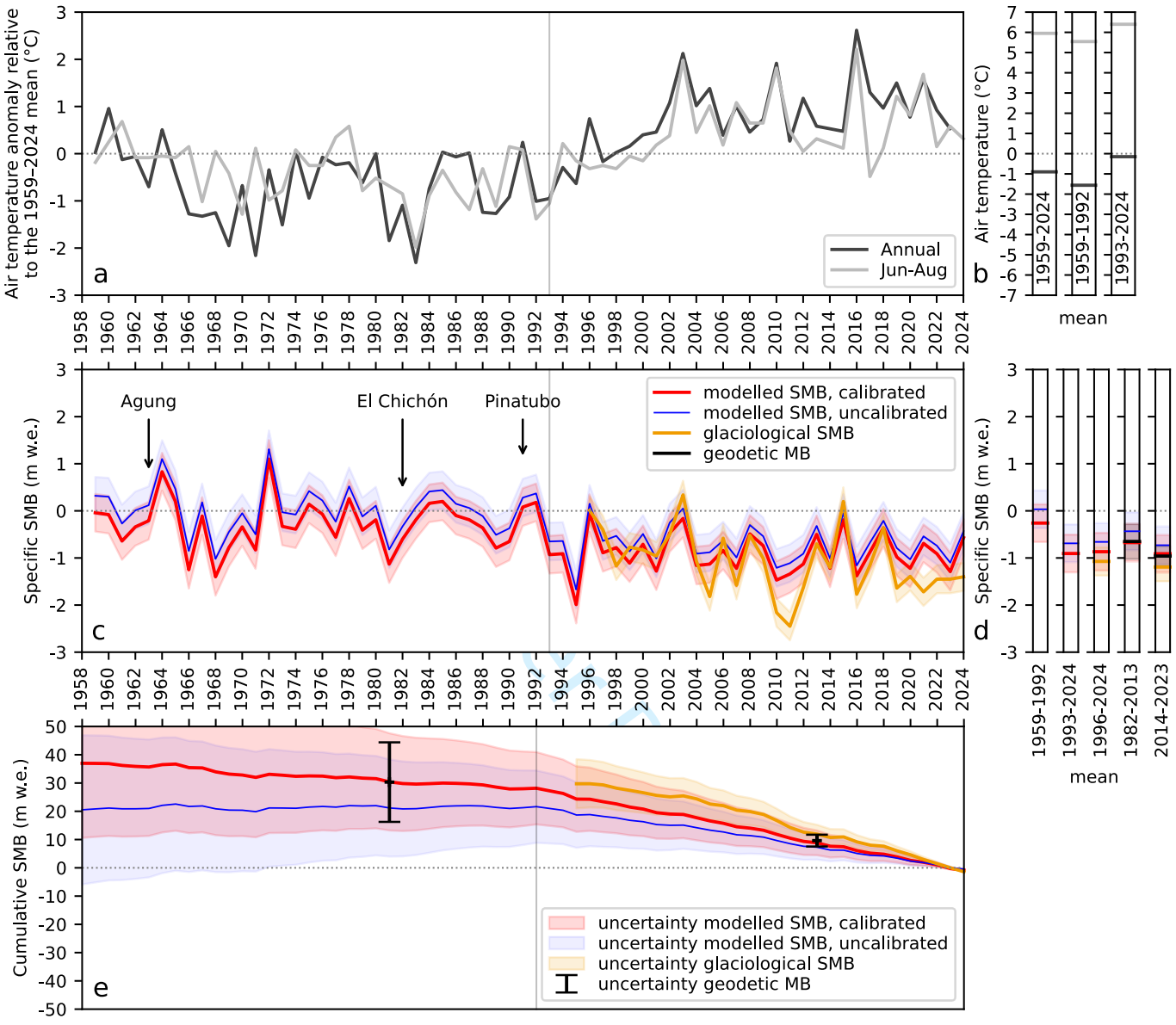

Fig. 5. a) Timeseries and b) averages of annual and summer Jun-Aug air temperature measured in Tasiilaq, 15 km southeast of MIT. c) Timeseries and d) averages of specific SMB, and e) cumulative SMB from the glaciological, modelled, and geodetic method. The reconstructed cumulative SMB series are normalized to a reference value of zero in 2023, the final year with complete coverage across all methods. This allows for a direct visual comparison of the cumulative SMB evolution across the three methods. Note that the normalized value of zero in 2023 does not represent the glacier's cumulative SMB in that year but simply anchors all series to the year 2023. The calibrated modelled SMB indicates a more negative mass balance regime in 1993-2024 (-0.91 ± 0.40 m w.e. a^{-1}) compared to 1959-1992 (-0.26 ± 0.40 m w.e. a^{-1}), coinciding with a summer mean air temperature increase from 5.5 °C to 6.4 °C and an annual mean air temperature increase from -1.6 °C to and -0.1 °C. The period 2014-23, which is covered by all three methods, exhibits a mass change of -1.19 ± 0.30 m w.e. a^{-1} (glaciological SMB), -0.91 ± 0.40 m w.e. a^{-1} (calibrated modelled SMB), and -0.96 ± 0.21 m w.e. a^{-1} (geodetic MB). Reconstructions of cumulative SMB from the calibrated model output agree well with the geodetically reconstructed glacier mass back to 2013 and 1981, which also holds for the glaciological SMB back to 2013. Generally, modelled and geodetic estimates underestimate mass loss at MIT when compared to the glaciological record but lie within uncertainties. Global and regional atmospheric and meteorological extremes are well depicted in the SMB time series.

Table 1. Comparison of specific (surface) mass balance rates across the three methods and mean air temperature during selected periods. SMB and MB at MIT can be directly compared since solid ice discharge can be disregarded as MIT is a land-terminating glacier and non-surface MB contributions are typically of negligible magnitude (Kaser and others, 2003; Huss and others, 2009; Zemp and others, 2013).

	Specific (S)MB rate (m w.e. a^{-1})			Mean air temp. (°C) in Tasiilaq	
	Glaciological	Modelled	Geodetic	Annual	Jun-Aug
1959-1992		-0.26 ± 0.40		-1.6	5.5
1959-2024		-0.57 ± 0.40		-0.9	6.0
1982-2013		-0.67 ± 0.40	-0.65 ± 0.37	-0.8	5.9
1982-2023		-0.73 ± 0.40	-0.72 ± 0.33	-0.6	6.1
1993-2024		-0.91 ± 0.40		-0.1	6.4
1996-2024	-1.07 ± 0.30	-0.87 ± 0.40		0.0	6.5
2014-2023	-1.19 ± 0.30	-0.91 ± 0.40	-0.96 ± 0.21	0.3	6.7

The reconstructed surface mass balance series based on the calibrated model output captures events and years of climate extremes well (Fig. 5a,c). Aerosols introduced to the stratosphere by large volcanic eruptions may lead to surface cooling due to scattering of the incoming solar radiation back to space (Robock, 2020). Lower air temperature in turn leads to decreased summer melt and an increased annual mass balance. Anthropogenic influences and volcanic aerosols are the main drivers of global glacier mass changes between 1961 and 2005 (Zemp and Marzeion, 2021). The eruptions of Agung (Indonesia) in 1963, El Chichón (Mexico) in 1982, and Pinatubo (Philippines) in 1991 resulted in record-high, positive changes in global ice mass in the respective following years (Zemp and Marzeion, 2021). On a Greenland-wide scale, the years 1972 as well as the post-volcanic years 1983 (El Chichón) and 1992 (Pinatubo) feature unusually low mid-tropospheric pressure over Greenland. The coldest years between 1900 and 2010 rank 1972 as first (annual average temperature 4.1 °C) and the 'volcanic' years of 1983 and 1992 (both 4.6 °C) as third and fourth (Hanna and others, 2012). These events can also be observed in the temperature timeseries in Tasiilaq (Fig. 5a) and in the mass balance of MIT (Fig. 5c). Years with lowest GrIS runoff rank 1992 (after Pinatubo) as first (MIT: third highest SMB), 1964 (after Agung) as second (MIT: second highest SMB), 1983 (after El Chichón) as third (MIT: fifth highest SMB), and 1972 as fourth (MIT: highest SMB) (Hanna and others, 2012). Two out of three years with a positive SMB during the period 1996-2024 (i.e., 1996 and 2003) can be associated with unusually high winter precipitation and low mean summer temperatures, respectively (Mernild and others, 2011). The positive SMB in 2015 might be related to notably low summer (June-August) air temperatures (Hanna and others, 2020).

6.2 Temporal and spatial variability

The model output allows for both assessing temporal and elevation-dependent changes in SMB at MIT. For changes in SMB during the mass balance year (Fig. 5a), we present the uncalibrated model output since the calibrated output is a result of annual SMB calibration and therefore does not resolve monthly timescales. Each respective month experienced a SMB decrease when comparing the periods 1959-92 and 1993-2024, except December which exhibits a slight increase. Greatest decreases in SMB can be observed in the months of June (-0.18 m w.e.), July (-0.20 m w.e.), and August (-0.13 m w.e.). This indicates that increased mass loss at MIT revealed by the modelled output is driven by summer melting (Fig. 6a) which is in agreement with observed summer temperature increase (Fig. 5a,b). Regarding the altitudinal sections, the calibrated model SMB shows a decrease in

each elevation band (<200, 200-300, 300-400, 400-500, 500-600, 700-800, >800 m a.s.l.) between the two periods, ranging from -0.82 m w.e. to -0.71 m w.e., with most negative values in the highest elevation bands (Fig. 6b).

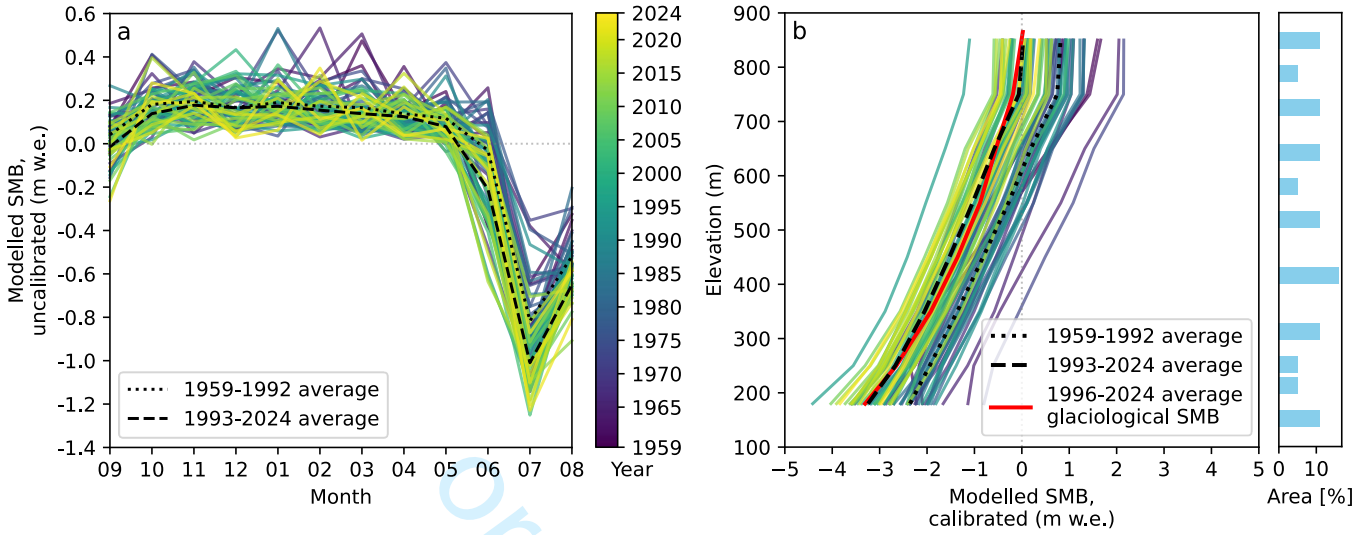

Fig. 6. Modelled SMB for a) each month and b) altitudinal sections during 1959-2024. SMB decreased in each month except December and most strongly during June-August as well as across the entire elevation range with largest decreases in the highest elevations.

The geodetic results highlight an altitudinal dependency of glacier surface elevation change (Fig. 7). Here we discuss elevation change rates as opposed to mass change rates, since the latter ones are estimated using an assumed glacier-wide density and utilizing a hypsometric interpolation for about 60 % of the surface area in the 1981 AERODEM. The maps show total surface lowering (Fig. 7a,b) and surface lowering rates (Fig. 7c,d) while maps including the 1981 data have major parts of the accumulation area masked out (Fig. 7a,c). These areas are affected by low contrast in the aerial photographs due to snow that prevents properly resolving heights masked out (Korsgaard and others, 2016b). Between 1981-2013 and 2013-23, virtually the entire glacier area experienced surface lowering (Fig. 7a,b). Pixel-wise surface change rates for 2013-23 are as low as -5.9 m a^{-1} (Fig. 7d), while the entire glacier surface lowered on average by 11.1 m during that time. A stronger surface lowering extends higher up the glacier in the recent period (Fig. 7d) compared to the period 1981-2013 (Fig. 7c), in line with observations of the snow line altitude at increasing elevations in satellite imagery and during field surveys (Mernild and others, 2013b). Increased surface lowering during 2013-23 between 600 and 800 m a.s.l. in the northern areas in contrast to the southern areas might be linked to the south-facing exposition (Fig. 7d). The lack of ablations stakes in these areas might explain why glaciological SMB are more negative than the modelled and geodetic estimates.

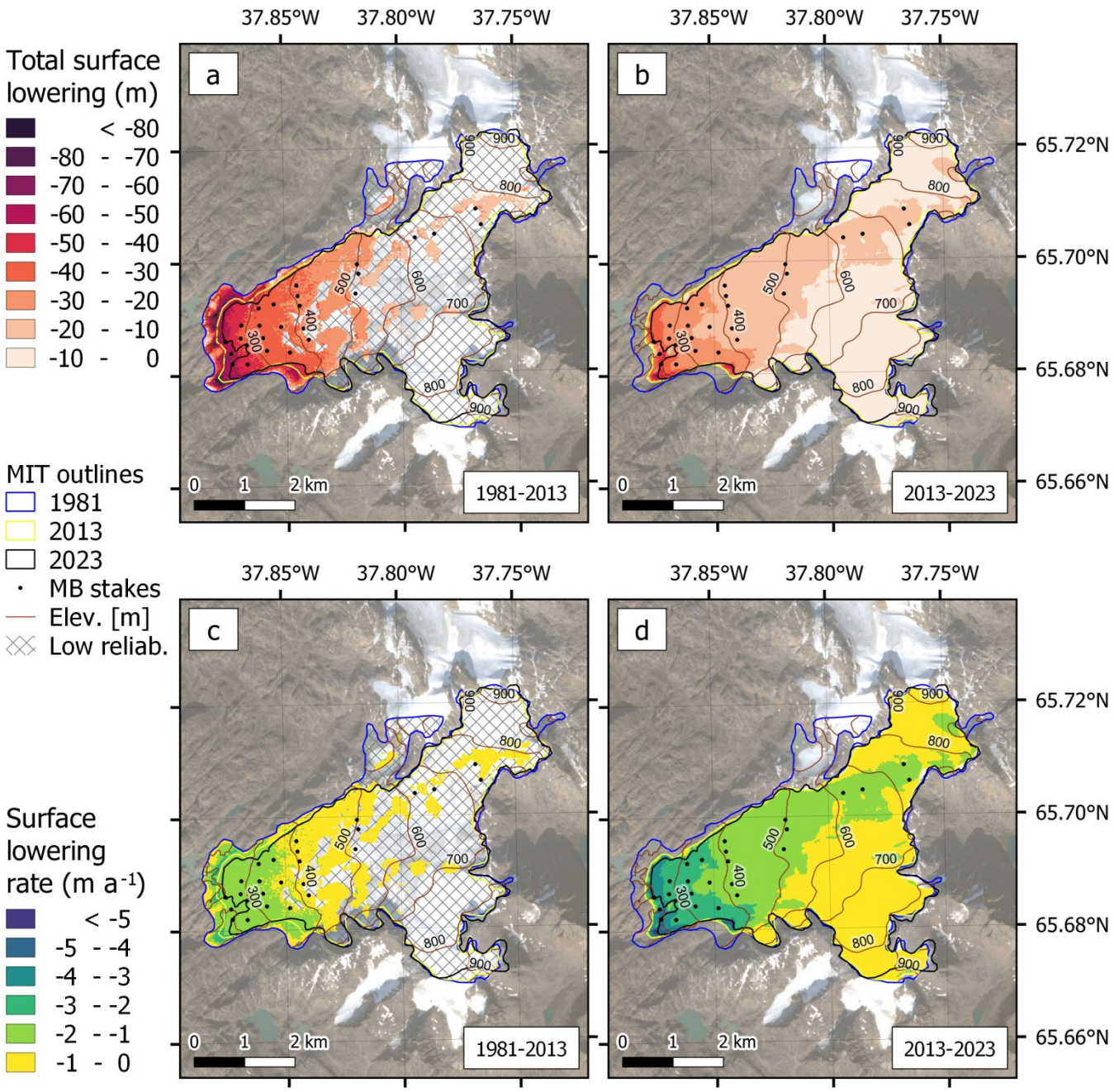

Fig. 7. a,b) Total surface lowering and c,d) surface lowering rate at MIT during the periods 1981-2013 and 2013-23, respectively. The 1981-2013 maps show only areas of high reliability in the AERODEM while low reliability areas are masked out. Those areas are accounted for in the geodetic MB by hypsometric interpolation. Over both periods the glacier surface area experienced surface lowering, with the largest losses in 2013-23. The greatest surface lowering rates are observed in the ablation area which are as low as -5.9 m a^{-1} during 2013-2023. Note that surface elevation changes for 1981-2013 and 2013-23 correspond to mass balances of 1982-2013 and 2014-23, respectively. Elevation contours are derived from Pléiades DEM in 2023 and glacier outlines are digitized from orthoimages of AERODEM and Pléiades DEM and from Landsat 7 imagery acquired on 20130803. Mass balance stakes that are currently part the glaciological mass balance programme are shown as black dots. Background image: S2 scene from 20230915 (ESA 2025).

6.3 Climate context

The air temperature record in Tasiilaq shows that mean summer and annual air temperatures have been increasing throughout the last decades (Fig. 5a-b, Table 1). When compared to temperature trends across larger regions with data available as recent as 2021 (Rantanen and others, 2022), Tasiilaq shows to be warming faster than the global mean but slower than the Arctic on average. Between 1959-92 and 1993-2021, the annual air temperature warming trend in Tasiilaq increased by 0.7 °C from -0.1 °C dec^{-1} to 0.6 °C dec^{-1}. During the same period, the annual air temperature warming trend increased globally by 0.5 °C from -0.3 °C dec^{-1} to 0.2 °C dec^{-1} and across the Arctic by 1.7 °C from -0.8 °C dec^{-1} to 0.9 °C dec^{-1} – which is more than three times the global trend (Rantanen and others, 2022). This points to MIT being far out of balance for the current climatological conditions which raises the question of the dominant driver of mass loss at MIT. Annual estimates of modelled SMB correlate moderately with summer air temperatures (Fig. 8a: $r = -0.39$, $p < 0.01$) and correlate more strongly with winter precipitation (Fig. 8b: $r = 0.51$, $p < 0.01$) observed in Tasiilaq. This shows that mass loss at MIT is driven by both increasing air temperatures and decreasing snowfall which has been discussed in studies before (e.g., Mernild and others, 2011). This is in line with a general trend of increasing summer temperatures and decreasing winter precipitation across coastal Greenland (Bjørk and others, 2018; Hanna and others, 2021).

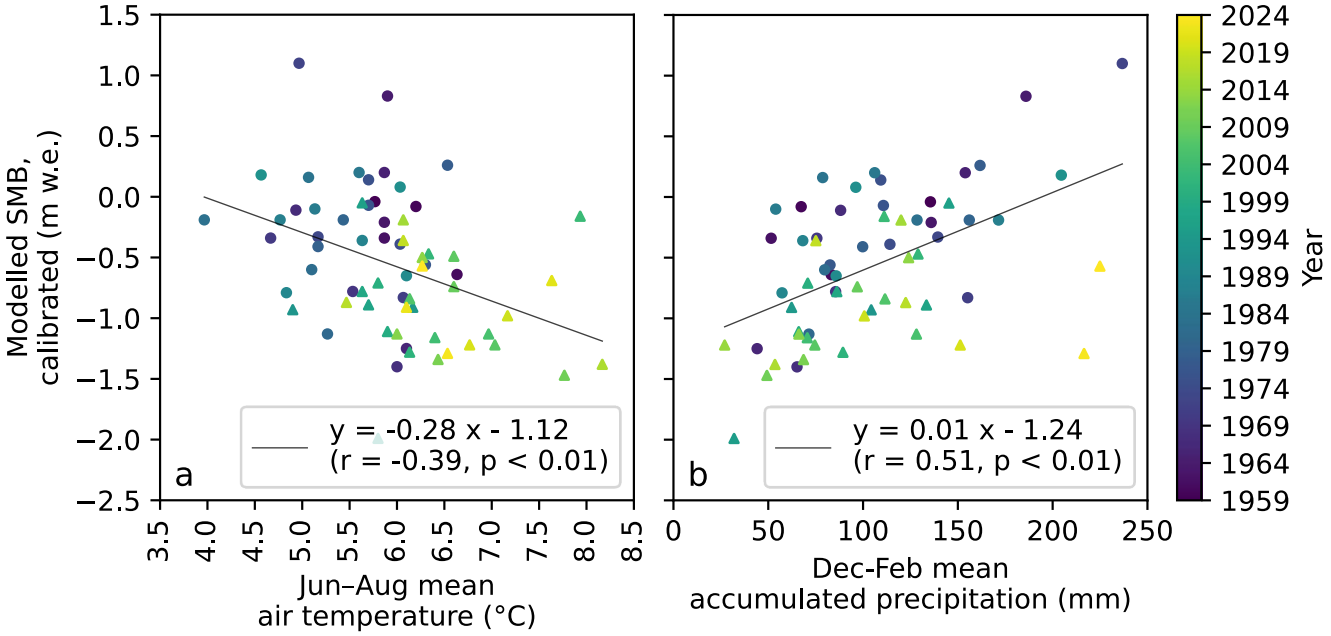

Fig. 8. Calibrated modelled SMB vs. a) Jun-Aug mean air temperature, exhibiting a moderate linear relationship ($r = -0.39$, $p < 0.01$) and b) Dec-Feb mean accumulated precipitation, exhibiting a strong linear relationship ($r = 0.51$, $p < 0.01$). Circles represent years during 1959-92 and triangles represent years during 1993-2024. Meteorological data was acquired by the weather station in Tasiilaq, 15 km southeast of MIT (Danish Meteorological Institute, 2026).

The interannual variability of SMB at MIT driven by summer air temperatures and winter precipitation can be linked to the larger-scale variability of climate. The calibrated, modelled SMB at MIT exhibits a positive relationship with the NAO index (Fig. 9a: $r = 0.38$, $p < 0.01$) and negative relationships with the GBI (Fig. 9b: $r = -0.47$, $p < 0.01$), the AMO index (Fig. 6c: $r = -0.49$, $p < 0.01$), and SST anomalies (Fig. 9d: $r = -0.24$, $p = 0.06$), being significant for the first three indices (significance level $\alpha = 0.01$). Years since 1993 exhibit strong positive GBI values, AMO index values, and SST anomalies (Fig. 9, Fig. S7)

which are indicative of their (multi-)decadal variability. At the GrIS, record high runoff years in the 1990s and 2000s can be associated with oceanic temperature forcing as gauged through the AMO (Hanna and others, 2012). Hanna and others (2012) state that record-warm Atlantic waters may have amplified the GrIS melt and runoff, which might also be the case for MIT (Fig. 9 c,d, Fig. S7) given its oceanic location and its proximity to the ocean (Fig. 1,S1). Furthermore, Greenland air temperatures and GrIS runoff over the last 30-40 years are strongly correlated with GBI anomalies (Hanna and others, 2012), which can be also observed at MIT. Positive GBI values have been coinciding with negative SMB since the late 1990s (Fig 6b). As air temperature and precipitation anomalies are influenced by the NAO and the GBI (Hanna et al., 2012), the temperature and precipitation variability observed in the MIT region can be linked to climate variability across a larger scale.

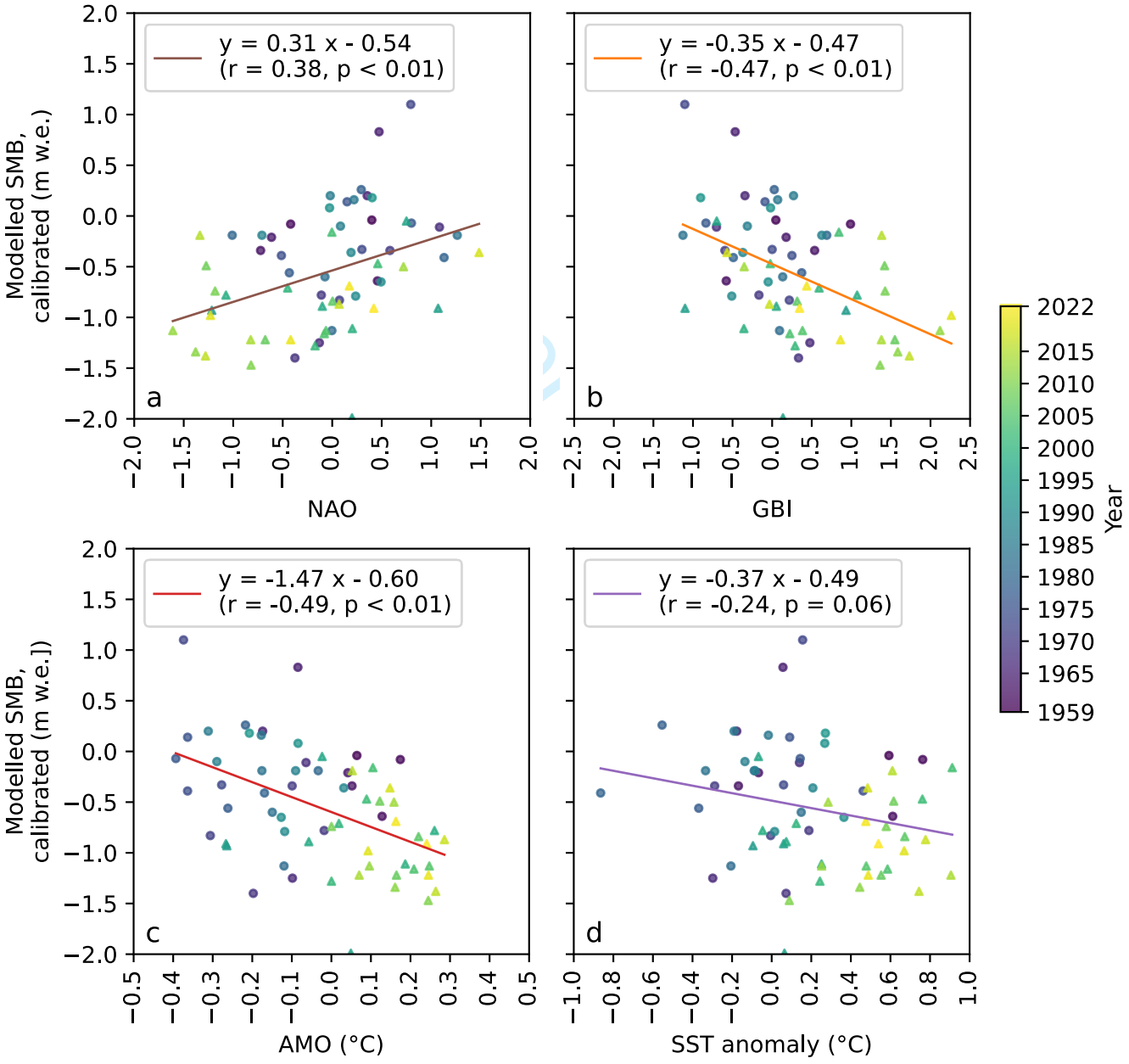

Fig. 9. Calibrated model SMB vs. four climate indices: a) North Atlantic Oscillation (NAO) index, b) Greenland Blocking Index (GBI), c) Atlantic Multidecadal Oscillation (AMO) index, and d) Sea Surface Temperature (SST) anomalies. Circles represent years during 1959-92 and triangles represent years during 1993-2022. The modelled SMB positively and negatively

correlates with climate indices with medium strength, being significant (significance level α = 0.01) for the NAO index, GBI, and AMO index. The GBI, AMO index, and SST anomalies exhibit increased values since the mid-1990s.

7. DISCUSSION

7.1 Limitations and potential

The comparison of (surface) mass balance records in this study is based on the following assumptions: (I) The reference area for the glaciological method has been adjusted only once throughout the record, meaning that a continuous glacier area decrease has not been accounted for in the annual estimates. The modelled SMB estimates are based on a fixed glacier geometry (elevation and extent), but are calibrated to account for past glacier extents, while the geodetic MB is based on discrete glacier outlines which are manually derived from satellite imagery. We tested the sensitivity of MB estimates in all three methods by varying the reference areas and found no significant changes or differences. Therefore, we assume that mass rate differences stemming from the differences in reference model glacier area and the actual glacier area are negligible. (II) The glaciological estimates are based on ablation stake measurements that have been typically conducted in the last two weeks of August with no specified timing, while the specific estimates of the modelled output are calculated from monthly cumulative values of SMB. The geodetic mass balances are based on image acquisitions which are not aligned to a specific day of the year, either due to unspecified dates (AERODEM, July/August 1981) or different acquisition dates (ArcticDEM on 20130730 and Pléiades DEM on 20230809/10). However, since the difference in temporal coverage of the mass balance estimates is in the order of a few days, we assume this temporal influence to be small. (III) Several studies suggest that englacial and subglacial mass loss processes are of negligible magnitude and are therefore not included in mass balance estimates (Kaser and others, 2003; Huss and others, 2009; Zemp and others, 2013). We also follow this assumption and therefore directly compare estimates of glaciological and model-derived SMB with MB estimates from the geodetic method.

The reconstructed evolution of specific surface mass balance at MIT from modelled data shows two distinct periods, i.e., 1959-92 and 1993-2024, with mass loss having more than tripled when comparing their respective SMB rates. The increased negative regime in recent decades is supported by the glaciological record covering 1996-2024 and by the geodetic MB results covering 2014-23. The calibrated model output underestimates SMB compared to the glaciological SMB and geodetic MB during respective periods, however, all methods agree within uncertainties. RACMO estimates SMB from meteorological (reanalysis) data, multi-layer snow cover simulations, including an albedo scheme (Noël and others, 2018). Since the model output is a simulation of real-world conditions and is a statistically downscaled product typically applied on a Greenland-wide scale (Noël and others, 2019), the glaciological record and geodetic methods might capture mass changes at MIT more confidently. However, the glaciological record might be affected by a spatial bias due to the distribution and density of the stakes, especially in higher elevations (Fig. 1), whereas the geodetic mass estimate has about 60 % of its surface area interpolated by the hypsometric method (Fig. 1). Considering the shortcomings of each method, the results still provide valuable and relevant information on MIT mass changes, particularly on its inter-annual variability and multi-annual rates.

We acknowledge that estimating ablation is challenging in areas close to the glacier terminus, especially when considering a rapid front recession over complex topography. Our presented

calibration of the model output, which includes estimating SMB at former glacier extents, improves the agreement between the modelled SMB and both glaciological and geodetic records. A limitation of our modelled SMB reconstruction, however, is the lack of measurements for validation, especially for estimates quantified before the start of the glaciological record in 1996. Using improved, high-resolution models combined with enhanced and better spatio-temporal coverage of in-situ measurements bears great potential to capitalize on the existing studies of mass balance at MIT.

7.2 Cross comparison of mass balance rates

Our reconstructed model SMB estimates for 1959-2024 show reasonable magnitude when compared to estimates from previous studies at MIT (Fig. 10). The published SMB estimates stem from studies using a variety of methods, including estimates from synoptic meteorological data, elevation changes from topographical maps, ablation stake data from both prior the initialization and as part of the glaciological mass balance programme, georadar studies, geodetic data, AWS data, and from estimates combining mass balance stake and geodetic data. The following two features must be considered for the comparison shown in Fig. 10: (I) The SMB estimate from Mernild and others (2008a) covers 1898-1993 and is compared to modelled SMB estimates for 1959-93. (II) The SMB estimate from the AWS site at MIT (Fausto and others, 2020) represents point SMB as opposed to the glacier-wide, specific SMB and is therefore compared to the modelled SMB estimate of the closest grid cell to the AWS site.

Our calibrated modelled SMB agrees well with previous MIT mass balance estimates. Differences between our and other published SMB can be explained by respective uncertainties in most of the studies. This highlights that our calibrated modelled SMB is robust to reconstruct mass loss at MIT. Mernild and others (2011) suggested that MIT is significantly out of balance with the current climate and will likely lose at least 70 % of its area and 80 % of its volume even in the absence of further climate warming. Because of their lagged response, glaciers will continue to lose mass at least for several decades even if global temperature is stabilized (IPCC, 2021). Therefore, projections of a continued air temperature increase (IPCC, 2021) will inevitably lead to sustained mass loss at MIT throughout this and the next century. Our study underlines that MIT is out of balance with the current climate. The increased mass loss at MIT from 1959-92 to 1993-2024 agrees with an observed mass loss acceleration across the Greenland periphery (Zemp and 14 others, 2019; Dussailant and others, 2025; The GlaMBIE Team, 2025).

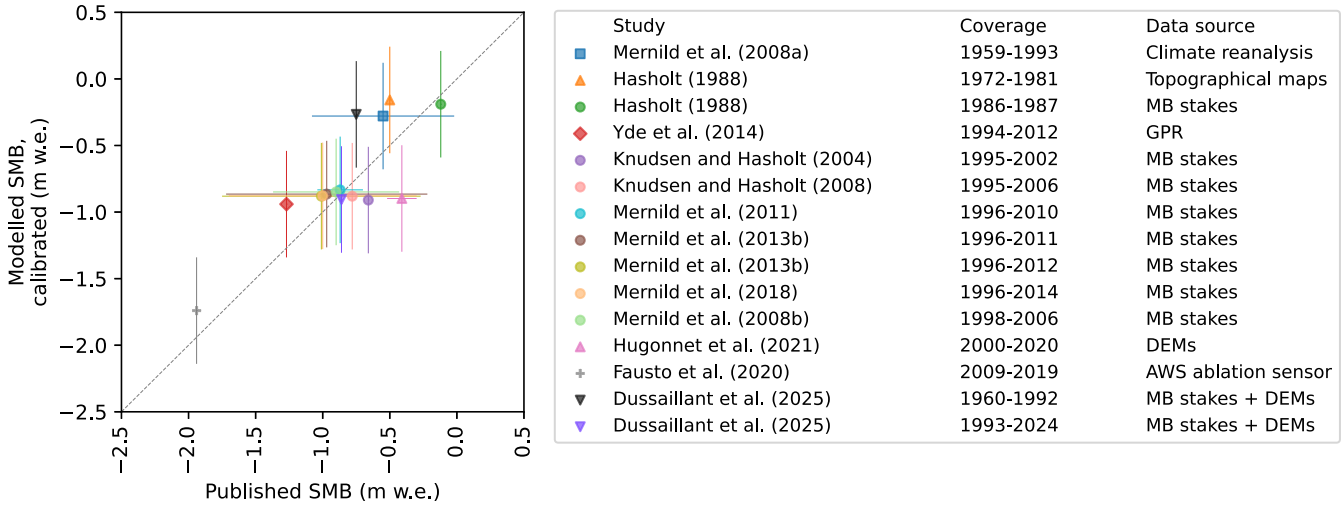

Fig. 10. Calibrated modelled SMB of our study vs. SMB estimates from previous studies at MIT during respective periods. Differences between the calibrated model output and previous SMB estimates can be accounted for by uncertainties in all estimates except for 1960-1992 from Dussaillant et al. (2025).

8. CONCLUSION

In this study, we demonstrate that estimates from glaciological, modelled, and geodetic methods compare well, allowing for reliably reconstructing mass balance at MIT back to 1959, i.e., prior to the initialization of the glaciological SMB programme in 1995. The three methods agree on (surface) mass balance estimates during 2014-23 being increasingly negative compared to the period before 2013 and show that MIT is out of balance with the current climate. During 1996-2024, which corresponds to the temporal coverage of the glaciological record, both the glaciological record and the modelled output show increased mass losses. The modelled SMB reconstruction shows that MIT tipped into a more negative mass balance regime from 1959-92 to 1993-2022 with a tripling of mass loss, coinciding with increased air temperatures and decreased winter precipitation. This is consistent with increased mass losses across peripheral Greenland since the early 1990s. Modelled SMB correlates with climate indices NAO, GBI, and AMO, showcasing that mass balance at MIT that is driven by changes in the local climate can be linked to a larger-scale climate variability. The modelled SMB also agrees with the magnitude of previously published estimates of SMB at MIT.

DATA AVAILABILITY

The mass balance estimates from our study can be found at https://doi.org/10.5281/zenodo.17550861.

SUPPLEMENTARY MATERIAL

The supplementary material for this article can be found at https://doi.org/10.5281/zenodo.17551030.

AUTHOR CONTRIBUTION STATEMENT

CP and JA designed the study. CP performed the analysis and wrote the manuscript. CP, SdV, KHS, JCY, JA, MKG, and NTK were involved in the glaciological data collection. BN provided the RACMO data. SdV, KHS, JCY, JA, WS, AAB, and BN provided critical feedback to the analysis. All authors reviewed and approved the final version of the manuscript.

ACKNOWLEDGEMENTS

B. Noël is a Research Associate of the Fonds de la Recherche Scientifique de Belgique – F.R.S.-FNRS. The Pléiades images/DEMs were provided by the Pléiades Glacier Observatory initiative of the French Space Agency (CNES) and Laboratoire d'Etudes en Géophysique et Océanographie Spatiales (LEGOS). The authors acknowledge the financial support from the University of Graz and from the EU Horizon 2020 project INTERACT III for the Transnational Access funding of the fieldwork (Grant Agreement No 871120).

REFERENCES

Barnston AG and Livezey RE (1987) Classification, seasonality and persistence of low-frequency atmospheric circulation patterns. *Mon. Wea. Rev.*, 115, 1083-1126 (doi: 10.1175/1520-0493(1987)115<1083:CSAPOL>2.0.CO;2)

Berthier E and 9 others (2023) Measuring glacier mass changes from space – a review. *Rep. Prog. Phys.*, 86, 036801 (doi: 10.1088/1361-6633/acaf8e)

Berthier E and 6 others (2024) Pléiades Glacier Observatory Data Products, EOST Collection (doi: 10.25577/313a-a978)

Beyer RA, Alexandrov O and McMichael S (2018) The Ames Stereo Pipeline: NASA's open source software for deriving and processing terrain data. *Earth and Space Science*, 5, 537-548 (doi: 10.1029/2018EA000409)

Bjørk AA and 13 others (2018). Changes in Greenland's peripheral glaciers linked to the North Atlantic Oscillation. *Nature Climate Change*, 8(1), 48-52 (doi: 10.1038/s41558-017-0029-1)

Box JE and 6 others (2018) Global sea-level contribution from Arctic land ice: 1971-2017. *Environ. Res. Lett.*, 13, 125012 (doi: 10.1088/1748-9326/aaf2ed)

Capellen J and Jensen DC (2021) Climatological Standard Normals 1991-2020 – Greenland, The Climate of Greenland - with Climatological Standard Normals, 1991-2020, DMI Report, 21-12. Danish Meteorological Institute, Copenhagen

Carrivick JL and 11 others (2023) Mass Loss of Glaciers and Ice Caps Across Greenland Since the Little Ice Age. *Geophys. Res. Lett.*, 50(10), e2023GL103950 (doi: 10.1029/2023GL103950)

CNES (2024a) PLEIADES, Two satellites to observe Earth close up. https://pleiades.cnes.fr/en/PLEIADES/index.htm, last access: 17 May 2024

CNES (2024b) demcompare. https://github.com/CNES/demcompare/blob/master/docs/source/index.rst, last access: 27 May 2024

Deschamps-Berger C and 7 others (2020) Snow depth mapping from stereo satellite imagery in mountainous terrain: evaluation using airborne laser-scanning data. The Cryosphere, 14(9), 2925-2940 (doi: 10.5194/tc-14-2925-2020)

Danish Meteorological Institute (2026) Climate Data. https://www.dmi.dk/friedata/dokumentation/climate-data, last access: 9 March 2026

Dussaillant I and 6 others (2025) Annual mass change of the world's glaciers from 1976 to 2024 by temporal downscaling of satellite data with in situ observations. *Earth Syst. Sci. Data*, 17(5), 1977-2006 (doi: 10.5194/essd-17-1977-2025)

ECMWF (2024a) ECMWF Reanalysis - 40 years (ERA-40). https://www.ecmwf.int/en/forecasts/dataset/ecmwf-reanalysis-40-years, last access: 6 May 2024

ECMWF (2024b) ECMWF Reanalysis - Interim (ERA-Interim). https://www.ecmwf.int/en/forecasts/dataset/ecmwf-reanalysis-interim, last access: 6 May 2024

ECMWF (2024c) ECMWF Reanalysis v5 (ERA5). https://www.ecmwf.int/en/forecasts/dataset/ecmwf-reanalysis-v5, last access: 6 May 2024

ECMWF-IFS (2008) Part IV: PHYSICAL PROCESSES (CY33R1), Technical Report. European Centre for Medium-Range Weather Forecasts, Reading (doi: 10.21957/8o7vwlbdr)

Enfield DB, Mestas-Nuñez AM and Trimble PJ (2001) The Atlantic Multidecadal Oscillation and its relation to rainfall and river flows in the continental U.S. *Geophysical Research Letters*, 28(10), 2077-2080 (doi: 10.1029/2000GL012745)

ESA (2024) Copernicus DEM - Global and European Digital Elevation Model (COP-DEM), GLO-30: worldwide coverage. https://spacedata.copernicus.eu/collections/copernicus-digital-elevation-model#C4, last access: 20 May 2024

ESA (2025) Sentinel-2. https://www.esa.int/Applications/Observing_the_Earth/Copernicus/Sentinel-2, last access: 10 July 2025

Ettema J, van den Broeke MR, van Meijgaard E, van de Berg WJ, Box JE and Steffen K (2010) Climate of the Greenland ice sheet using a high-resolution climate model – Part 1: Evaluation. *The Cryosphere*, 4, 511-527 (doi: 10.5194/tc-4-511-2010)

Fausto RS, Abermann J and Ahlstrøm AP (2020) Annual surface mass balance records (2009–2019) from an automatic weather station on Mittivakkat Glacier, SE Greenland. *Front. Earth Sci.*, 8, 251, (doi: 10.3389/feart.2020.00251)

Fristrup B (1960) Studies of Four Glaciers in Greenland. *Geografisk Tidsskrift*, 59

Fristrup B (1970) Ny geografisk station i Grønland. *Geografisk Tidsskrift*, 69(2), 192-203

Hanna E and 6 others (2012) The influence of North Atlantic atmospheric and oceanic forcing effects on 1900-2010 Greenland summer climate and ice melt/runoff. *International Journal of Climatology*, 33(4) 862-880 (doi: 10.1002/joc.3475)

Hanna E, Cropper TE, Hall RJ and Cappelen J (2016) Greenland Blocking Index 1851–2015: A regional climate change signal. *International Journal of Climatology*, 36(15), 4847-4861 (doi: 10.1002/joc.4673)

Hanna E and 8 others (2021) Greenland surface air temperature changes from 1981 to 2019 and implications for ice-sheet melt and mass-balance change. *Int J Climatol*, 41 (doi: 10.1002/joc.6771)

Hansche I, Shahi S, Abermann J and Schöner W (2023) The vertical atmospheric structure of the partially glacierised Mittivakkat valley, southeast Greenland. *Journal of Glaciology*, 69(277), 1097-1108 (doi: 10.1017/jog.2022.120)

Hasholt B (1986) Kortlægning af Mitdluagkat Gletscheren og nogle hydro-glaciologiske observationer. *Geografisk Tidsskrift*, 86, 9-16

Hasholt B (1987) A new map of the Mitdluagkat glacier - a preliminary report. *Geografisk Tidsskrift*, 87, 19-21

Hasholt B (1988) Massbalance studies of the Mitdluagkat Glacier, Eastern Greenland. *Geografisk Tidsskrift*, 88, 82-85

Hasholt B and Jakobsen, B.H., 2013. 75 years of research at the Sermilik Station: 1933-2008. Geografisk Tidsskrift, 108(1) (doi: 10.1080/00167223.2008.10649571)

Hasholt B, van As D and Knudsen NT (2016) Historical ablation rates on south-east Greenland glaciers measured in the 1933 warm summer. *Polar Research*, 2016, 35, 28858 (doi: 10.3402/polar.v35.28858)

Hugonnet R and 10 others (2021) Accelerated global glacier mass loss in the early twenty-first century. *Nature*, 592, 726-731 (doi: 10.1038/s41586-021-03436-z)

Huss M (2013) Density assumptions for converting geodetic glacier volume change to mass change. *The Cryosphere*, 7, 877-887 (doi:10.5194/tc-7-877-2013)

Huss M, Bauder A and Funk M (2009) Homogenization of long-term mass-balance time series. *Annals of Glaciology*, 50, 50, 198-206 (doi: 10.3189/172756409787769627)

Huss M, Dhulst L and Bauder A (2017) New long-term mass-balance series for the Swiss Alps. *Journal of Glaciology*, 61, 227, 551-562 (doi: 10.3189/2015JoG15J015)

IPCC (2019) The Ocean and Cryosphere in a Changing Climate. In Pörtner HO and 12 others eds. *Special Report of the Intergovernmental Panel on Climate Change*, Cambridge University Press, Cambridge (doi: 10.1017/9781009157964)

IPCC (2021) Climate Change 2021: The Physical Science Basis. In Masson-Delmotte V and 17 others eds. *Sixth Assessment Report of the Intergovernmental Panel on Climate Change*, Cambridge University Press, Cambridge (doi: 10.1017/9781009157896)

IPCC (2022) Climate Change 2022: Impacts, Adaptation and Vulnerability. In Pörtner HO and 11 others eds. *Sixth Assessment Report of the Intergovernmental Panel on Climate Change*, Cambridge University Press, Cambridge (doi: 10.1017/9781009325844)

Kaplan A, Cane MA, Kushnir Y, Clement AC, Blumenthal MB and Rajagopalan B (1998) Analyses of global sea surface temperature 1856–1991. *Journal of Geophysical Research Oceans*, 103(C9), 18567-18589 (doi: 10.1029/97JC01736)

Kaser G, Fountain A and Jansson P (2003) A manual for monitoring the mass balance of mountain glaciers. *IHP-VI Technical Documents in Hydrology*, 59, UNESCO-IHP, Paris

Kääb A (2008) Glacier Volume Changes Using ASTER Satellite Stereo and ICESat GLAS Laser Altimetry. A Test Study on Edgeøya, Eastern Svalbard. *IEEE Transaction on Geoscience and Remote Sensing*, 46, 10, 2823-2830 (doi: 10.1109/TGRS.2008.2000627)

Kääb A and 11 others (2005) Remote sensing of glacier- and permafrost-related hazards in high mountains: an overview. *Nat. Hazards Earth Syst. Sci.*, 5, 527-554 (doi: 10.5194/nhess-5-527-2005)

745 Khan SA and 8 others (2022) Accelerating Ice Loss From Peripheral Glaciers in North Greenland.
746 *Geophys. Res. Lett.*, 49(12), e2022GL098915 (doi: 10.1029/2022GL098915)

747 Kjeldsen K and 15 others (2015) Spatial and temporal distribution of mass loss from the Greenland
748 Ice Sheet since AD 1900. *Nature*, 528, 396-400 (doi: 10.1038/nature16183)

749 Knudsen NT and Hasholt B (1999) Radio-echo Sounding at the Mittivakkat Gletscher, Southeast
750 Greenland. *Arctic, Antarctic, and Alpine Research*, 31, 3, 321-328 (doi: 10.2307/1552263)

751 Knudsen NT and Hasholt B (2004) Mass balance observations at Mittivakkat Gletscher, Southeast
752 Greenland 1995–2002. *Hydrology Research*, 35, 4, 381-390 (doi: 10.2166/nh.2004.0029)

753 Knudsen NT and Hasholt B (2008) Mass balance obsevations at Mittivakkat Glacier, Ammassalik
754 Island, Southeast Greenland 1995-2006. Geografisk Tidsskrift, 108, 1, 111-120 (doi:
755 10.1080/00167223.2008.10649577)

756 Knudsen NT, Nørnberg P, Yde JC, Hasholt B and Heinemeier J (2008) Recent marginal changes of the
757 Mittivakkat Glacier, Southeast Greenland and the discovery of remains of reindeer (Rangifer
758 tarandus), polar bear (Ursus maritimus) and peaty material. *Geografisk Tidsskrift*, 108, 1, 137-142 (doi:
759 10.1080/00167223.2008.10649579)

760 Korsgaard NJ and 6 others (2016a) Digital Elevation Model and orthophotographs of Greenland based
761 on aerial photographs from 1978-1987 (G150 AERODEM) (NCEI Accession 0145405), NOAA National
762 Centers for Environmental Information (doi: 10.7289/v56q1v72)

763 Korsgaard NJ and 6 others (2016b) Digital elevation model and orthophotographs of Greenland based
764 on aerial photographs from 1978–1987. *Sci Data*, 3, 160032 (doi: 10.1038/sdata.2016.32)

765 Kuipers Munneke P, van den Broeke MR, Lenaerts JTM, Flanner MG, Gardner AS and van de Berg WJ
766 (2011) A new albedo parameterization for use in climate models over the Antarctic ice sheet. *J.*
767 *Geophys. Res.*, 116, D05114 (doi: 10.1029/2010JD015113)

768 Larocca LJ and 9 others (2023) Greenland-wide accelerated retreat of peripheral glaciers in the
769 twenty-first century. *Nature Climate Change*,13, 1324–1328 (doi: 10.1038/s41558-023-01855-6)

770 Lenaerts JTM and 6 others (2012) Modeling drifting snow in Antarctica with a regional climate model:
771 1. Methods and model evaluation. *J. Geophys. Res.-Atmos.*, 117, D05108 (doi: 10.1029/2011JD016145)

772 Maxar 2024. Maxar, EXPLORE, CONNECT, PROTECT. https://www.maxar.com/, last access: 16 May
773 2024

774 McNabb R, Nuth C, Kääb A and Girod L (2018) Sensitivity of glacier volume change estimation to DEM
775 void interpolation. *The Cryosphere*, 13, 895-910 (doi: 10.5194/tc-13-895-2019)

776 Mernild SH (2006) The internal drainage system of the lower Mittivakkat Glacier, Ammassalik Island,
777 SE Greenland. Geografisk Tidsskrift-Danish Journal of Geography, 106, 1, 13-24,
778 https://doi.org/10.1080/00167223.2006.10649542.

779 Mernild SH and Hasholt B (2006) Climatic control on river discharge simulations, Mittivakkat Glacier
780 catchment, Ammassalik Island, SE Greenland. *Hydrology Research*, 37, 4, 327-346 (doi:
781 10.2166/nh.2006.018)

782 Mernild SH, Liston GE, Hasholt B and Knudsen NT (2006a) Snow Distribution and Melt Modeling for
783 Mittivakkat Glacier, Ammassalik Island, Southeast Greenland. *Journal of Hydrometeorology*, 7, 4, 808-
784 824 (doi: 10.1175/JHM522.1)

785 Mernild SH, Hasholt B and Liston GE (2006b) Water flow through Mittivakkat Glacier, Ammassalik
786 Island, SE Greenland. *Geografisk Tidsskrift*, 106, 1, 25-43 (doi: 10.1080/00167223.2006.10649543)

787 Mernild SH, Kane DL, Hansen BU, Jakobsen BH, Hasholt B and Knudsen NT (2008a) Climate, glacier
788 mass balance and runoff (1993–2005) for the Mittivakkat Glacier catchment, Ammassalik Island, SE
789 Greenland, and in a long term perspective (1898–1993). *Hydrology Research*, 39, 4, 239-256 (doi:
790 10.2166/nh.2008.101)

791 Mernild SH, Liston GE, Kane DL, Knudsen NT and Hasholt B (2008b) Snow, runoff, and mass balance
792 modeling for the entire Mittivakkat Glacier (1998–2006), Ammassalik Island, SE Greenland. *Geografisk*
793 *Tidsskrift*, 108, 1, 121-136 (doi: 10.1080/00167223.2008.10649578)

794 Mernild SH, Hansen BU, Jakobsen BH, Hasholt B (2008c) Climatic conditions at the Mittivakkat Glacier
795 catchment (1994–2006), Ammassalik Island, SE Greenland, and in a 109-year perspective (1898–
796 2006). *Geografisk Tidsskrift*, 108, 1, 51-72 (doi: 10.1080/00167223.2008.10649574)

797 Mernild SH and 6 others (2011) Increasing mass loss from Greenland's Mittivakkat Gletscher. *The*
798 *Cryosphere*, 5, 341-348 (doi: 10.5194/tc-5-341-201)

799 Mernild SH and 7 others (2013a) Volume and velocity changes at Mittivakkat Gletscher, southeast
800 Greenland. *Journal of Glaciology*, 59, 216, 660-670 (doi: 10.3189/2013JoG13J017)

801 Mernild SH, Pelto M, Malmros JK, Yde JC, Knudsen NT and Hanna E (2013b) Identification of snow
802 ablation rate, ELA, AAR and net mass balance using transient snowline variations on two Arctic
803 glaciers. *Journal of Glaciology*, 59, 216, 649-659 (doi: 10.3189/2013JoG12J221)

804 Mernild SH and 8 others (2015a) Greenland precipitation trends in a long-term instrumental climate
805 context (1890-2012): evaluation of coastal and ice core records. *Int. J. Climatol.*, 35(2), 303-320 (doi:
806 10.1002/joc.3986)

807 Mernild SH and 7 others (2015b) Albedo decline on Greenland's Mittivakkat Gletscher in a warming
808 climate. *Int. J. Climatol.*, 35, 2294-2307 (doi: 10.1002/joc.4128)

809 Mernild SH, Beckerman AP, Knudsen NT, Hasholt B and Yde JC (2018) Statistical EOF analysis of
810 spatiotemporal glacier mass-balance variability: a case study of Mittivakkat Gletscher, SE Greenland.
811 Geografisk Tidsskrift, 118, 1, 1-16 (doi: 10.1080/00167223.2017.1386581)

812 Natural Earth, 2024. 1:10m Physical Vectors. https://www.naturalearthdata.com/downloads/10m-
813 physical-vectors/, last access: 19 May 2024.

NOAA CPC, 2024. North Atlantic Oscillation (NAO). https://www.cpc.ncep.noaa.gov/products/precip/CWlink/pna/nao.shtml, last access: 24 June 2024.

NOAA PSL, 2024a. Greenland Blocking Index (GBI). https://psl.noaa.gov/gcos_wgsp/Timeseries/GBI_UL/, last access: 24 June 2024.

NOAA PSL, 2024b. AMO (Atlantic Multidecadal Oscillation) Index. https://psl.noaa.gov/data/timeseries/AMO/, last access: 24 June 2024.

NOAA PSL, 2024c. Kaplan Extended SST V2. https://psl.noaa.gov/data/gridded/data.kaplan_sst.html, last access: 24 June 2024.

Noël B and 11 others (2018) Modelling the climate and surface mass balance of polar ice sheets using RACMO2 – Part 1: Greenland (1958–2016). *The Cryosphere*, 12, 811-831 (doi: 10.5194/tc-12-811-2018)

Noël B, van de Berg WJ, Lhermitte S and van den Broeke MR (2019) Rapid ablation zone expansion amplifies north Greenland mass loss. *Science Advances*, 5, eaaw0123 (doi: 10.1126/sciadv.aaw0123)

Noh MJ and Howat IM (2015) Automated stereo-photogrammetric DEM generation at high latitudes: Surface Extraction with TIN-based Search-space Minimization (SETSM) validation and demonstration over glaciated regions. *GIScience & Remote Sensing*, 52, 2, 198-217 (doi: 10.1080/15481603.2015.1008621)

Nuth C and Kääb A (2011) Co-registration and bias corrections of satellite elevation data sets for quantifying glacier thickness change. *The Cryosphere*, 5, 271-290 (doi: 10.5194/tc-5-271-2011)

Paul F, Winsvold SH, Kääb A, Nagler T and Schwaizer G (2016) Glacier Remote Sensing Using Sentinel-2, Part II: Mapping Glacier Extents and Surface Facies, and Comparison to Landsat 8. *Remote Sens.*, 2016, 8, 575 (doi: 10.3390/rs8070575)

PGC, 2024. PGC DEM Products – ArcticDEM, REMA, and EarthDEM. https://www.pgc.umn.edu/guides/stereo-derived-elevation-models/pgc-dem-products-arcticdem-rema-and-earthdem/, last access: 16 May 2024.

Porter C and 28 others (2018) ArcticDEM, Version 3. https://doi.org/10.7910/DVN/OHHUKH, last access: 16 May 2024.

PROMICE/GC-Net, 2024. Programme for monitoring of the Greenland Ice Sheet & Greenland Climate Network. https://promice.org/, last access: 5 May 2024.

QGreenland, 2024. QGreenland v2.0.0. https://nsidc.org/qgreenland/packages/v2.0.0/, last access: 19 May 2024.

Rantanen M and 7 others (2022) The Arctic has warmed nearly four times faster than the globe since 1979. *Commun. Earth Environ.*, 3, 168 (doi: 10.1038/s43247-022-00498-3)

Robock A (2020) Volcanic eruptions and climate. *Reviews of Geophysics*, 38, 2, 159-294 (doi: 10.1029/1998RG000054)

Shean D and 7 others (2021) dshean/demcoreg: v1.1.0. (doi: 10.5281/zenodo.5733347)

Silva T, Abermann J, Noël B, Shahi S, van de Berg WJ and Schöner W (2022) The impact of climate oscillations on the surface energy budget over the Greenland Ice Sheet in a changing climate. *The Cryosphere*, 16, 3375-3391 (doi: 10.5194/tc-16-3375-2022)

The GlaMBIE Team (2025) Community estimate of global glacier mass changes from 2000 to 2023. Nature, 639, 382–388 (doi: 10.1038/s41586-024-08545-z)

Undèn P and 25 others (2002) HIRLAM-5, Scientific Documentation, Technical Report, HIRLAM-5 Project. Swedish Meteorological and Hydrological Institute (SMHI), Norrköping

USGS, 2024. Landsat Collection 2, Level-1 Data. https://www.usgs.gov/landsat-missions/landsat-collection-2-level-1-data, last access: 28 May 2024.

van der Schot J, Abermann J, Silva T, Jensen CD, Noël B and Schöner W (2023) Precipitation trends (1958–2021) on Ammassalik island, south-east Greenland. *Front. Earth Sci.*, 10, 1085499 (doi: 10.3389/feart.2022.1085499)

van Meijgaard, E., van Ulft, L.H., van de Berg, W.J., Bosveld, F.C., van den Hurk, B., Lenderink, G., and Siebesma, A.P., 2008. Technical Report 302: The KNMI regional atmospheric climate model RACMO version 2.1. Royal Netherlands Meteorological Institute, De Bilt, Netherlands, 50pp.

WGMS, 2025. Fluctuations of Glaciers (FoG) Database Version 2025 (doi: 10.5904/wgms-fog-2025-02b)

Yde JC and 7 others (2014) Volume measurements of Mittivakkat Gletscher, southeast Greenland. *Journal of Glaciology*, 60, 224, 1199-1207 (doi: 10.3189/2014JoG14J047)

Zemp M and Marzeion B (2021) Dwindling relevance of large volcanic eruptions for global glacier changes in the Anthropocene. *Geophysical Research Letters*, 48, e2021GL092964 (doi: 10.1029/2021GL092964)

Zemp M and 16 others (2013) Reanalysing glacier mass balance measurement series. *The Cryosphere*, 7, 1227-1245 (doi: 10.5194/tc-7-1227-2013)

Zemp and 14 others (2019) Global glacier mass changes and their contributions to sea-level rise from 1961 to 2016. *Nature*, 568, 382-386 (doi: 10.1038/s41586-019-1071-0)